Part II:

Chapter 4. Macrotexture measurements

Measurement of pole figure

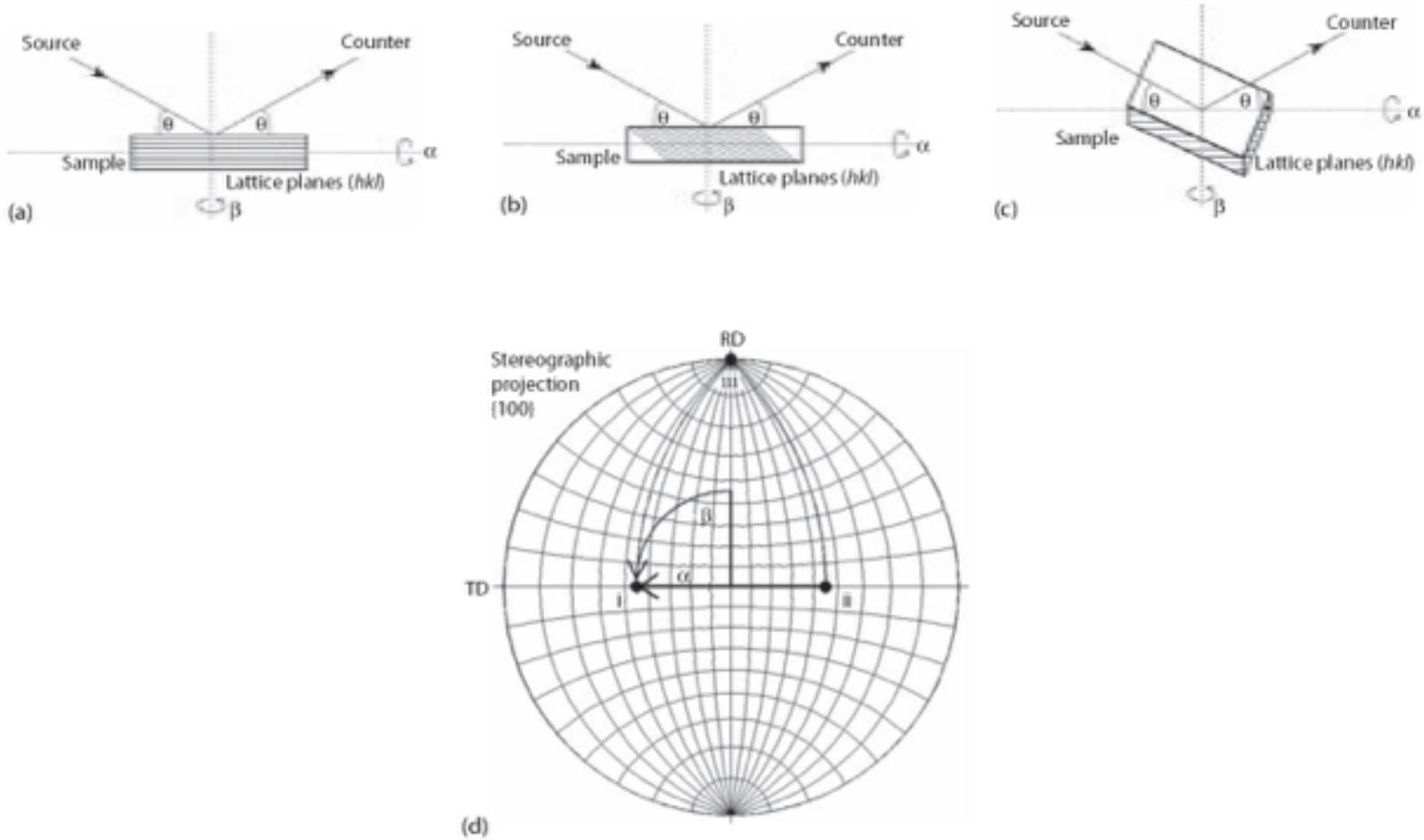

FIGURE 4.1
Sketch to illustrate the effect of sample rotation on the arrangement of the lattice planes and the resulting reflection conditions in a texture goniometer.

{111} pole figure of 97% cold-rolled Al

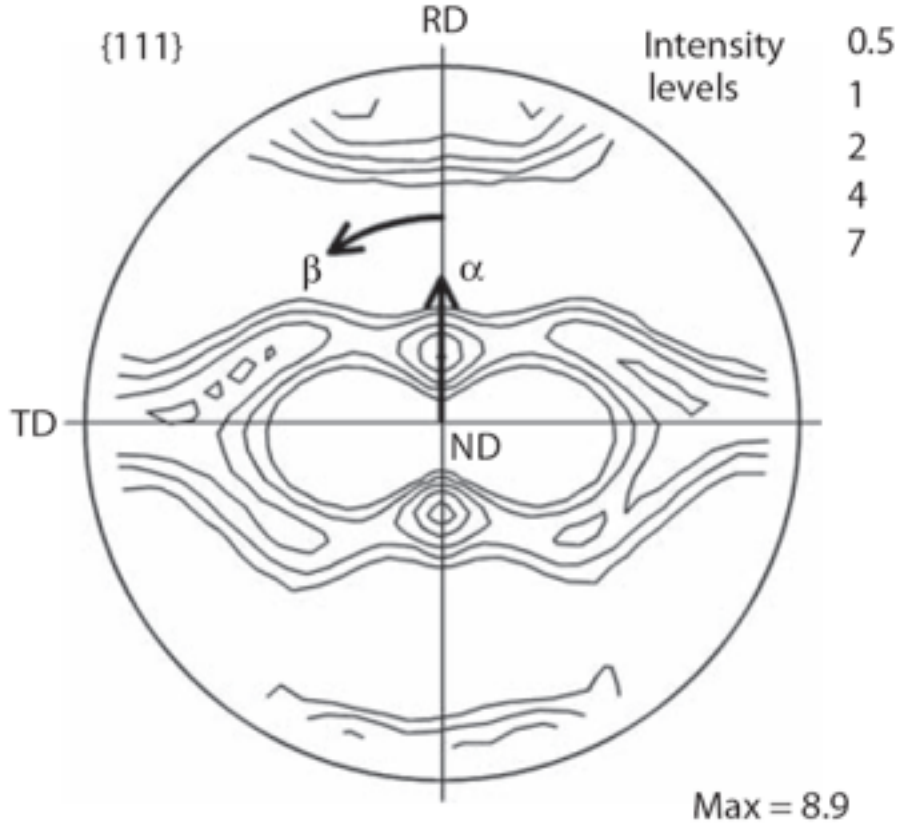

FIGURE 4.2
{111} Pole figure of 97% cold-rolled aluminum with the definition of the pole figure angles α and β. The orientation densities are given by iso-intensity lines in multiples of a random orientation distribution.

Geometry of texture goniometers

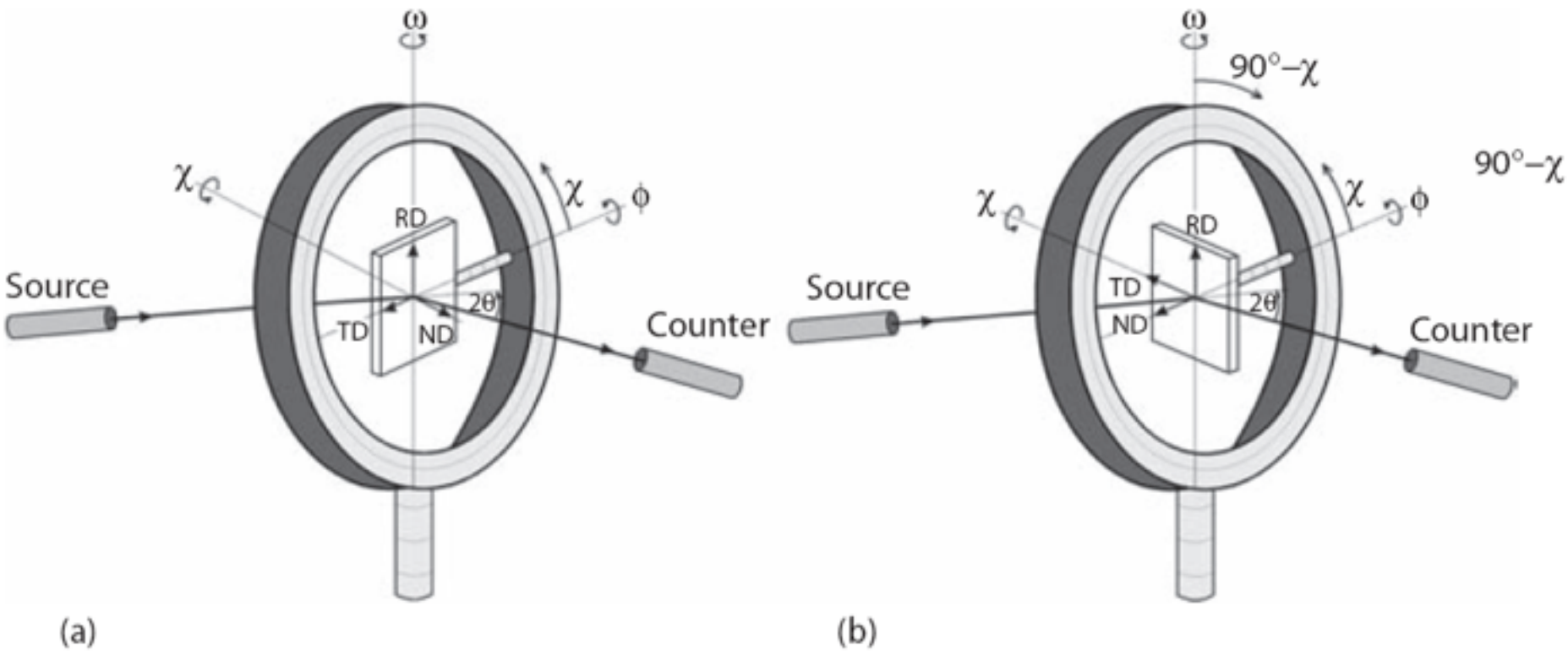

Setup of texture goniometers

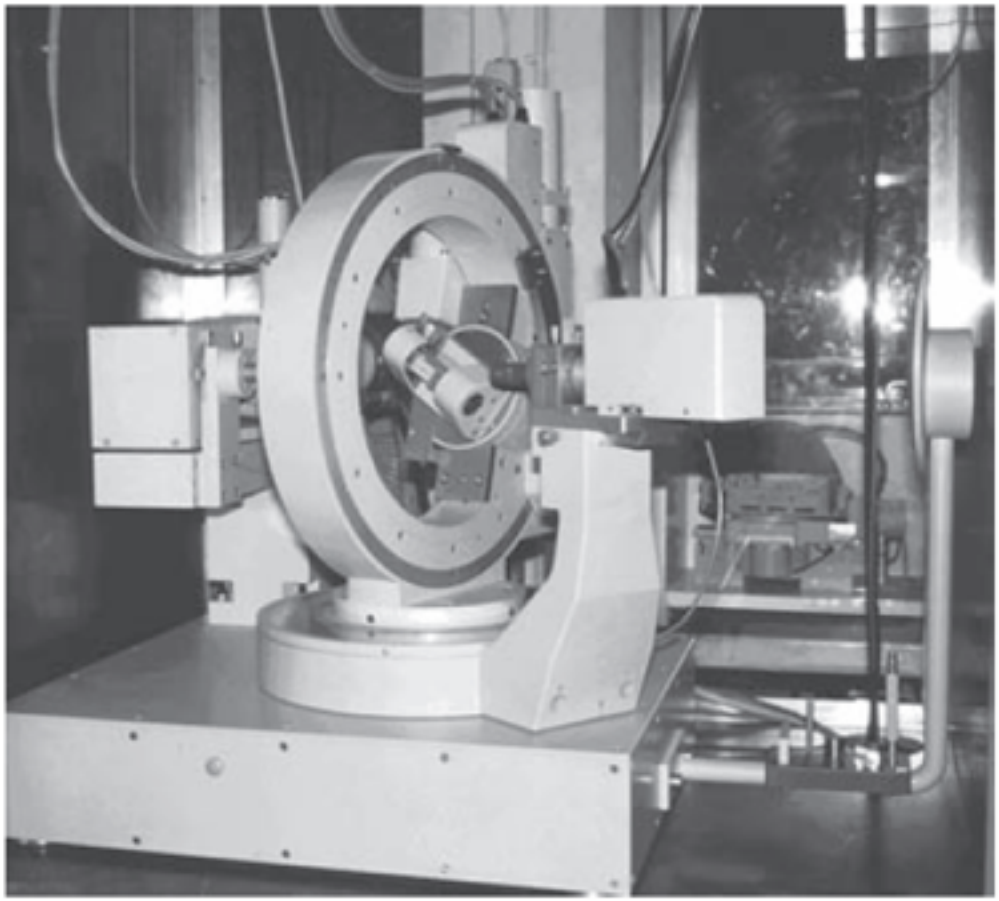

FIGURE 4.4
Texture goniometer at the Institut für Metallkunde und Metallphysik, RWTH Aachen.

Generation of X-ray

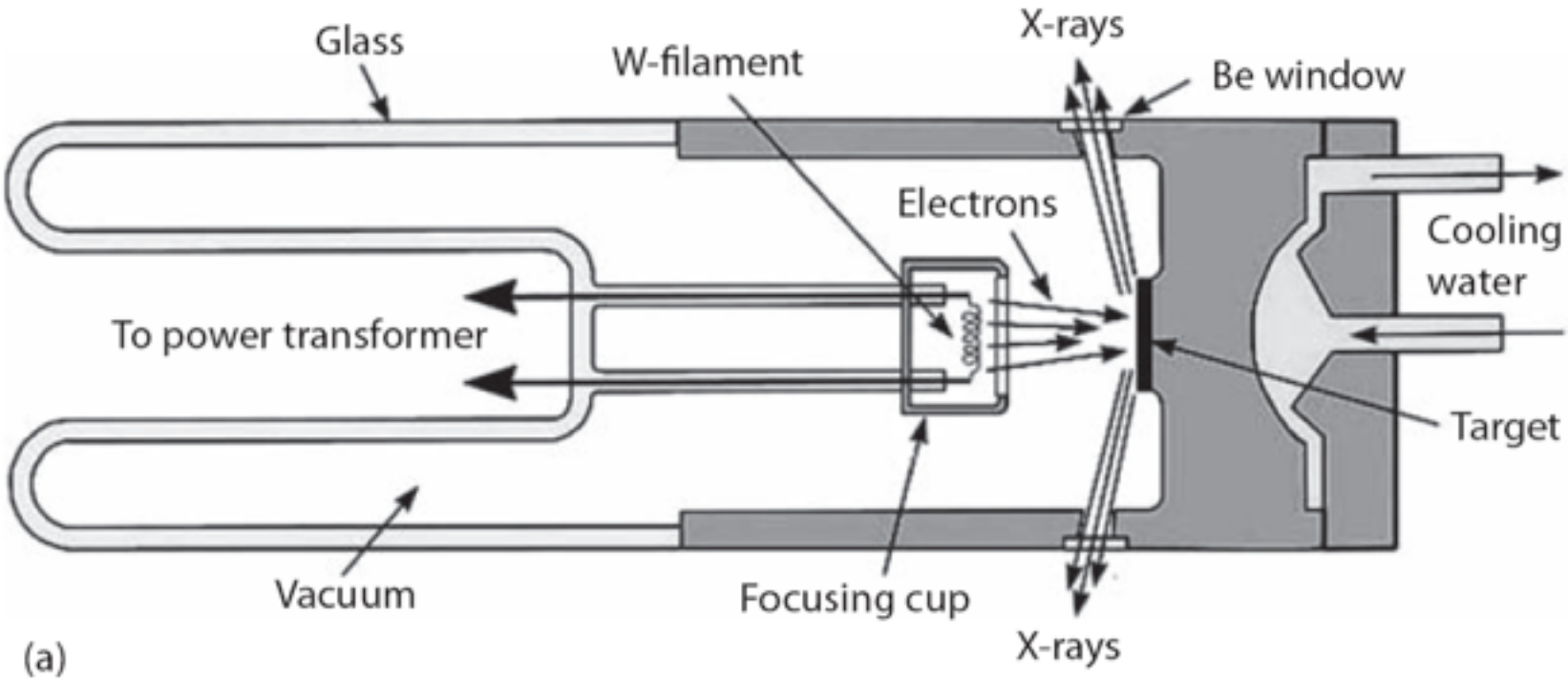

http://www.doitpoms.ac.uk/tlplib/xray-diffraction/production.php?printable=1

Emission spectrum of X-ray

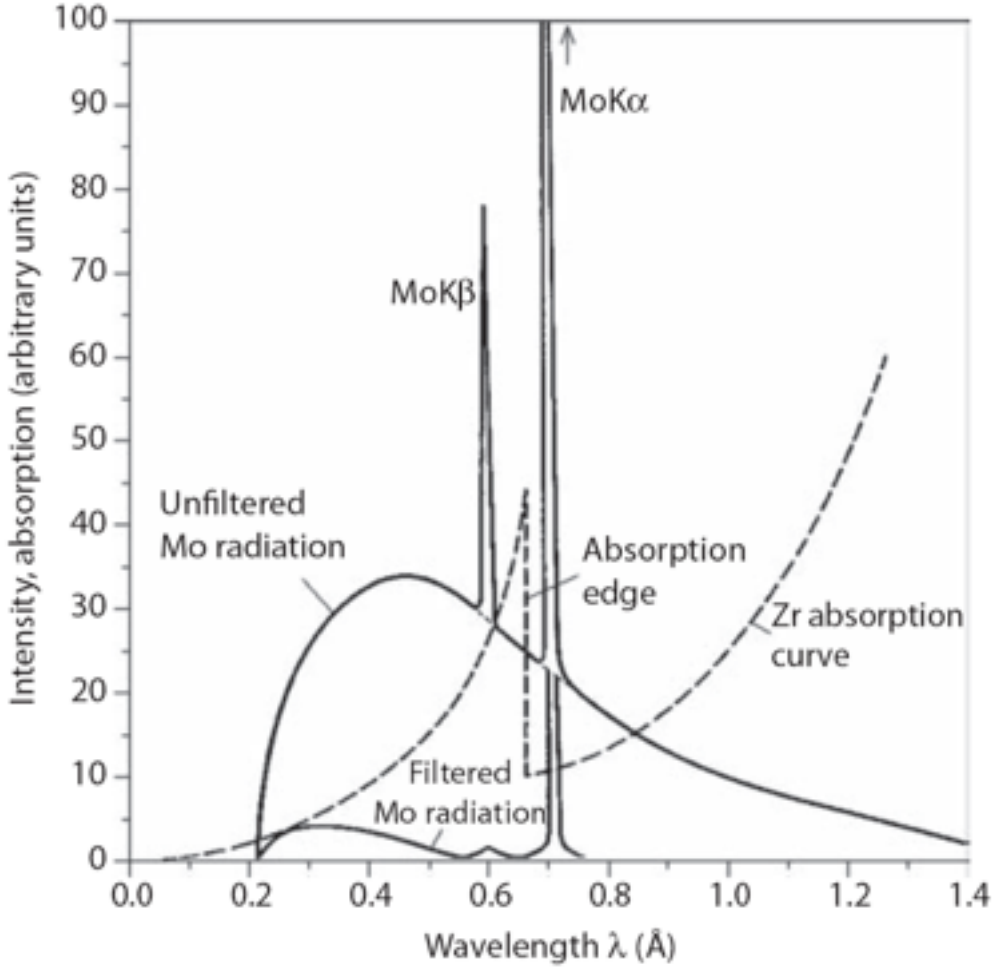

(b)

FIGURE 4.5
(a) Scheme of an x-ray tube for diffraction experiments and (b) emission spectrum of a molybdenum x-ray tube operating at 55 kV and absorption spectrum of a zirconium filter (see Figure 3.12).

Wavelengths and filters of X-ray

Table 4.1 Characteristics of various X-ray tubes and appropriate filters (data from Int. Tables for X-ray Crystallography, 1985)

	Wavelength [nm]		$K\beta$-filter			
Anode material	$K\alpha$	$K\beta$	Material	Edge wavelength [nm]	Thickness for $K\beta/K\alpha = 1:500$ [μm]	Loss in $K\alpha$ [%]
Cr	0.22909	0.20848	V	0 22690	17	51
Fe	0.19373	0.17565	Mn	0.18964	18	53
Co	0.17902	0.16208	Fe	0.17433	19	54
Cu	0.15418	0.13922	Ni	0.14880	23	60
Mo	0 07107	0.06323	Zr	0.06888	120	71
Ag	0.05609	0.04970	Rh	0.05338	90	73
			Pd	0.05092	92	74

Effect of filters: 1

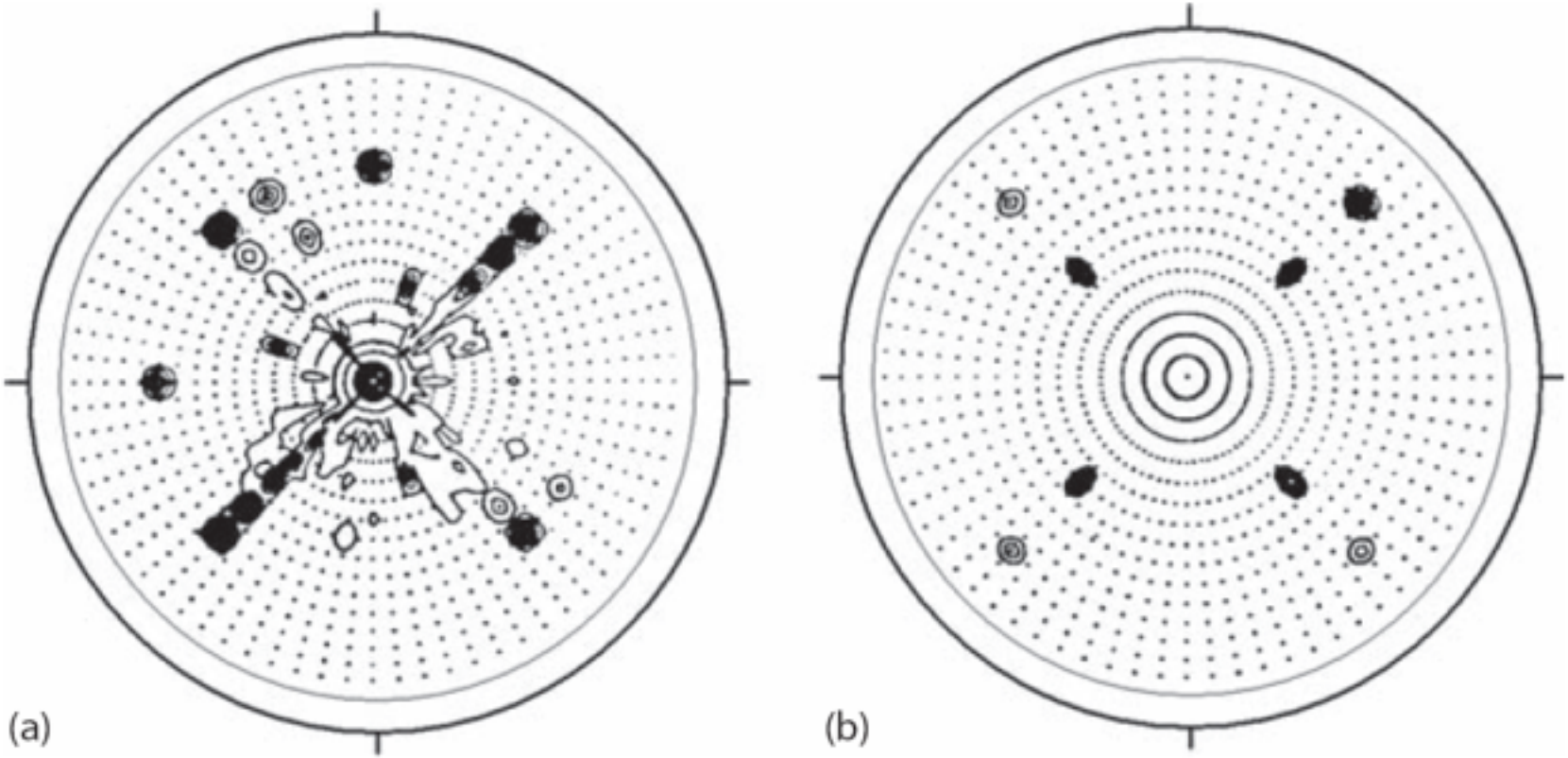

FIGURE 4.6
{102} Pole figure of a 400 nm YBaCuO film on a $LaAlO_3$ substrate measured with (a) Kβ-filtered CuKα radiation and (b) truly monochromatic CuKα radiation. Note additional peaks in (a) that are due to diffraction with different wavelengths on the substrate. (Courtesy of H.R. Wenk.)

Effect of filters: 2

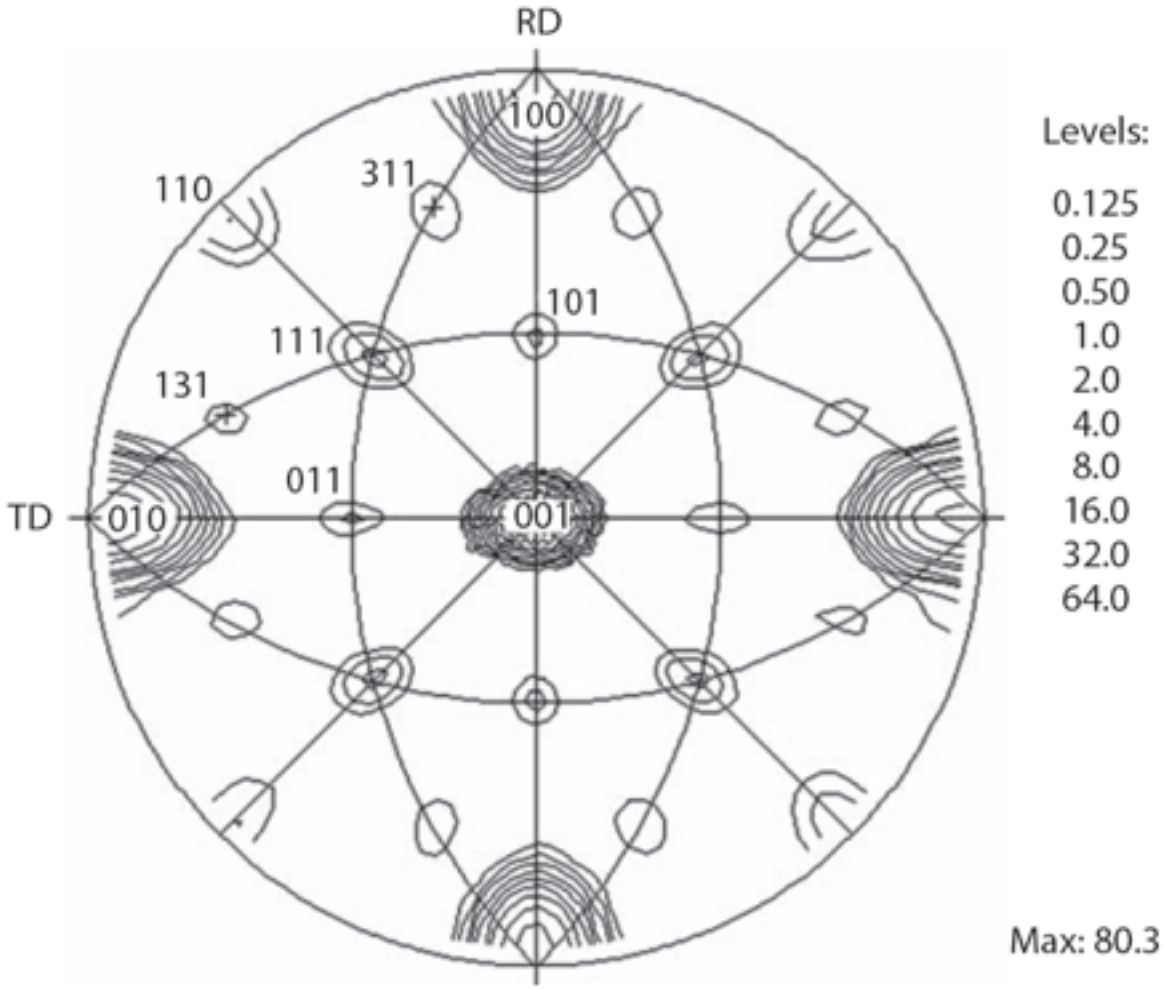

FIGURE 4.7
{200} Pole figure of highly textured aluminum foil, showing additional weak reflection peaks of nonmonochromatic radiation at different lattice planes.

Monochromatic radiation

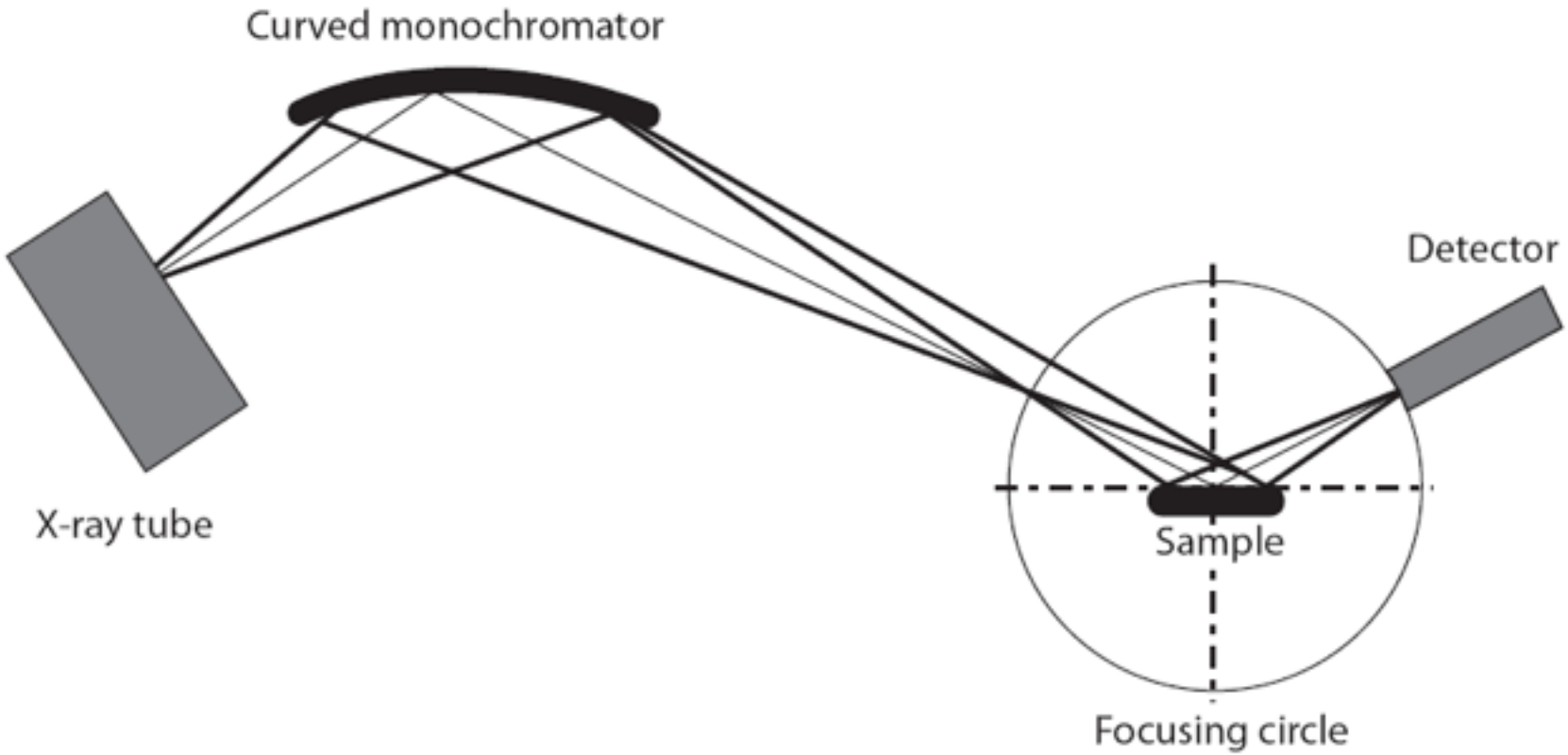

FIGURE 4.8
Principle of a curved monochromator in the primary beam path to produce monochromatic radiation.

Depth penetration

$$G_x = 1 - \exp\left(\frac{-2\mu x}{\sin\theta}\right)$$

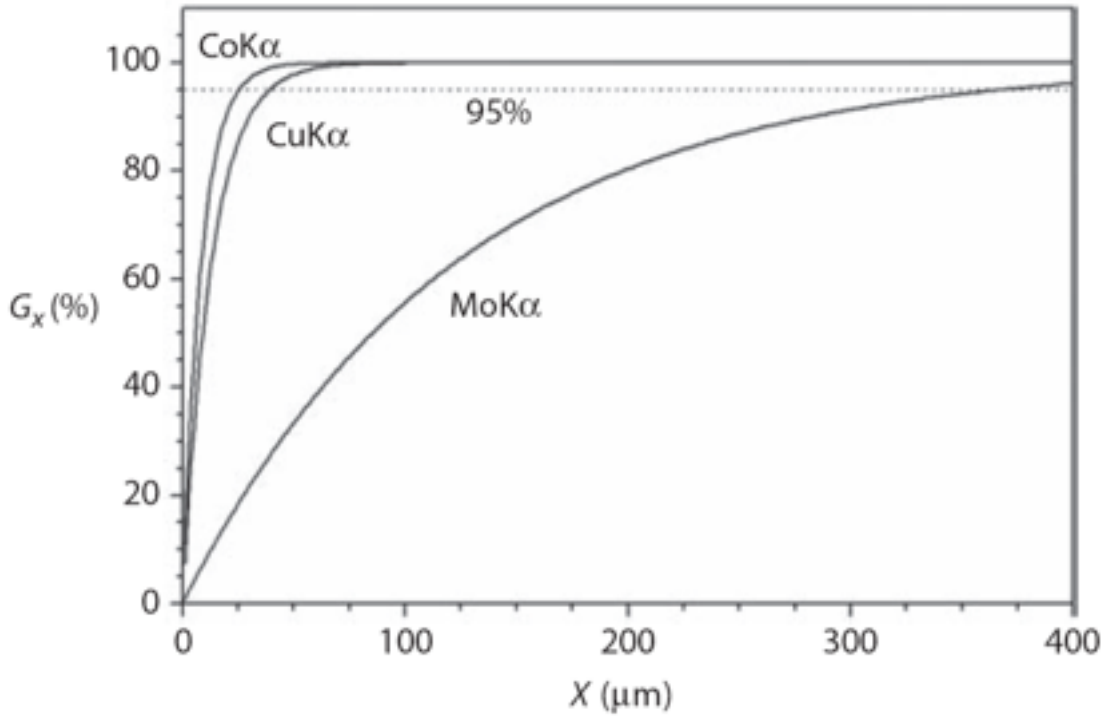

FIGURE 4.9
Evolution of G_x with depth x in aluminum for three different x-ray tubes (reflection angle $\theta = 20°$, normal incidence).

Depth penetration-cont.

TABLE 4.2

Depth x (in μm) That Leads to G_x Values of 95% for Different X-Ray Tubes and Materials Analyzed in Reflection Geometry at a Bragg Angle $\theta = 20°$

	CoKα	CuKα	MoKα
Al	25.4	39.1	368.0
Fe	12.3	2.1	16.9
Cu	7.0	10.8	11.2

Defocusing Error: Geometry Distortion

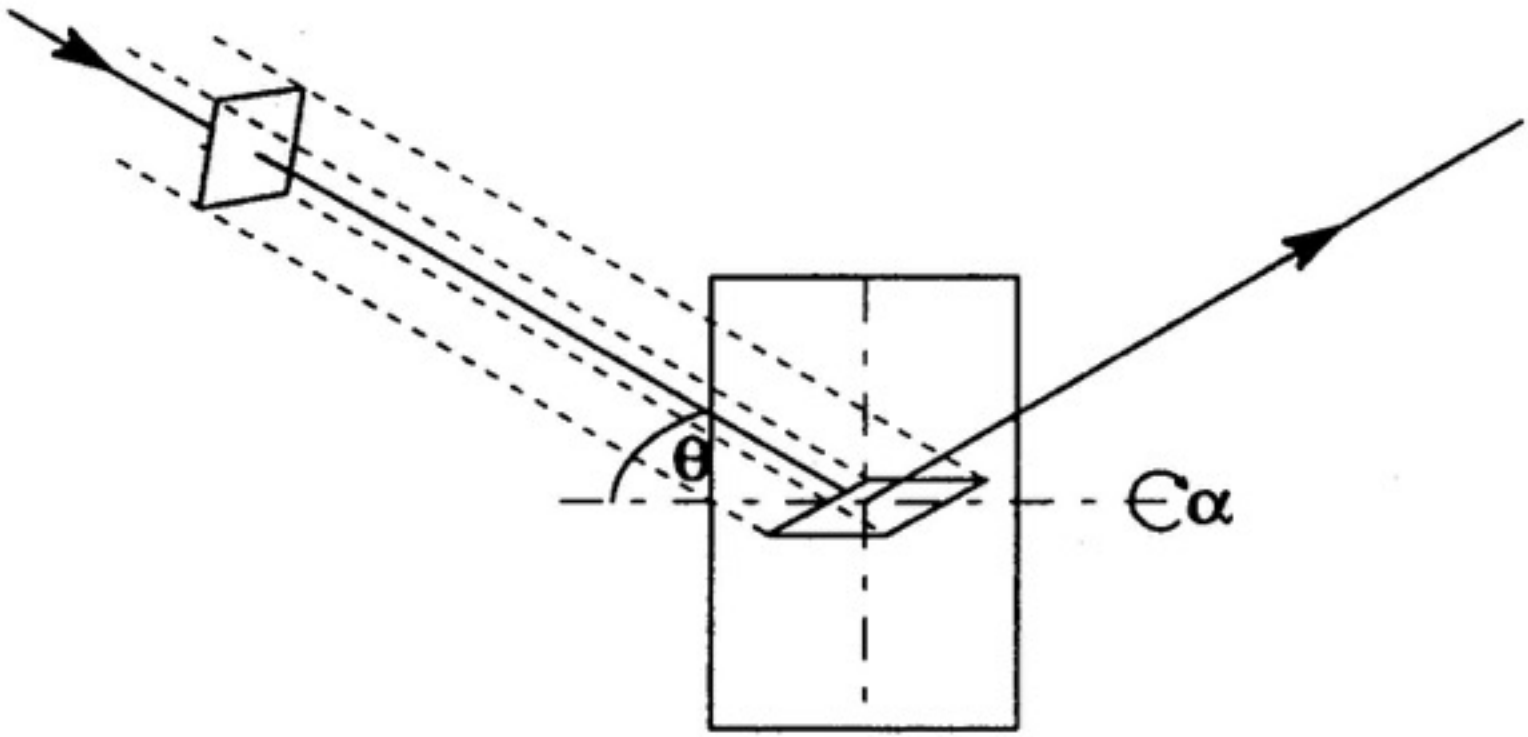

Geometry Distortion

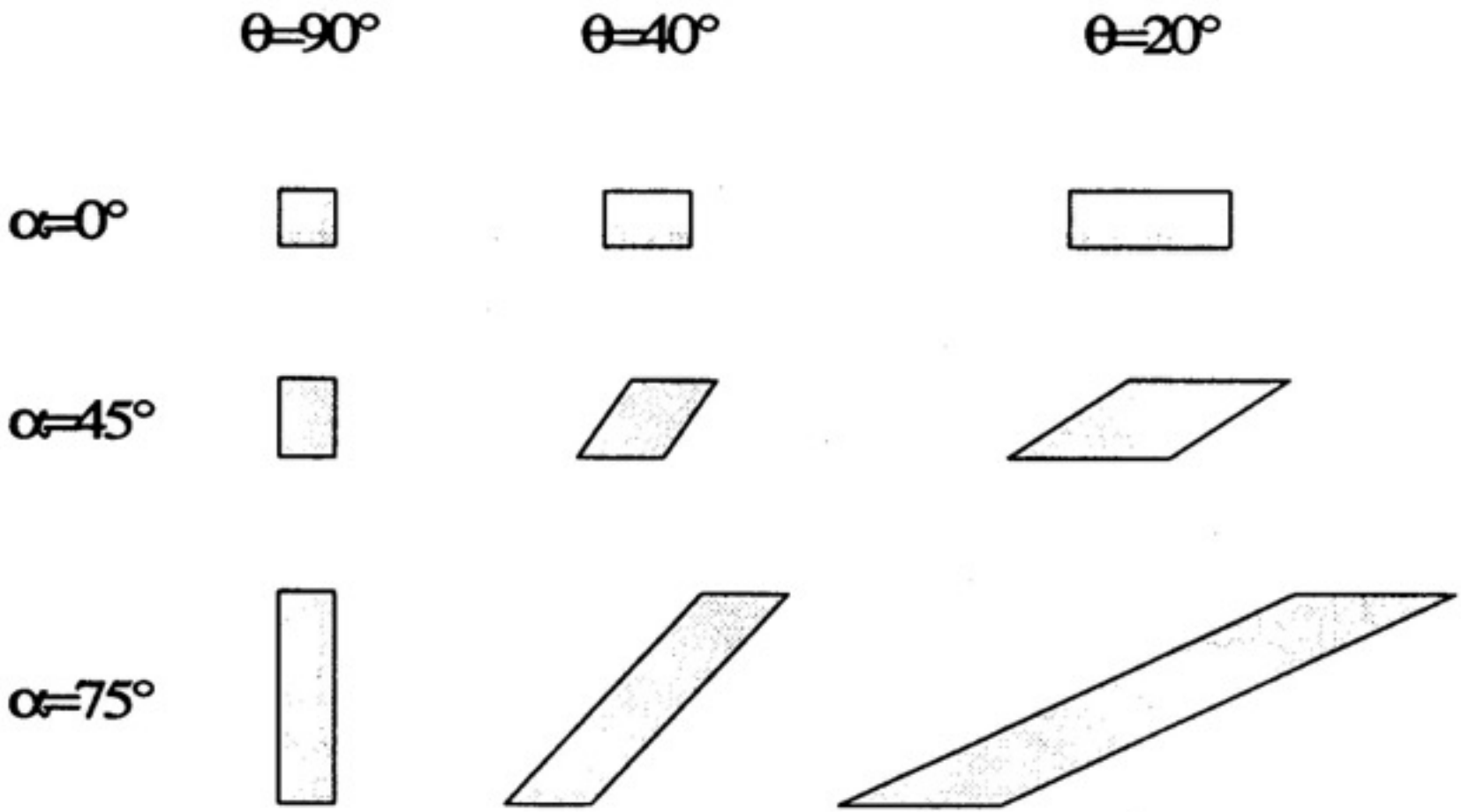

Peak Broadening

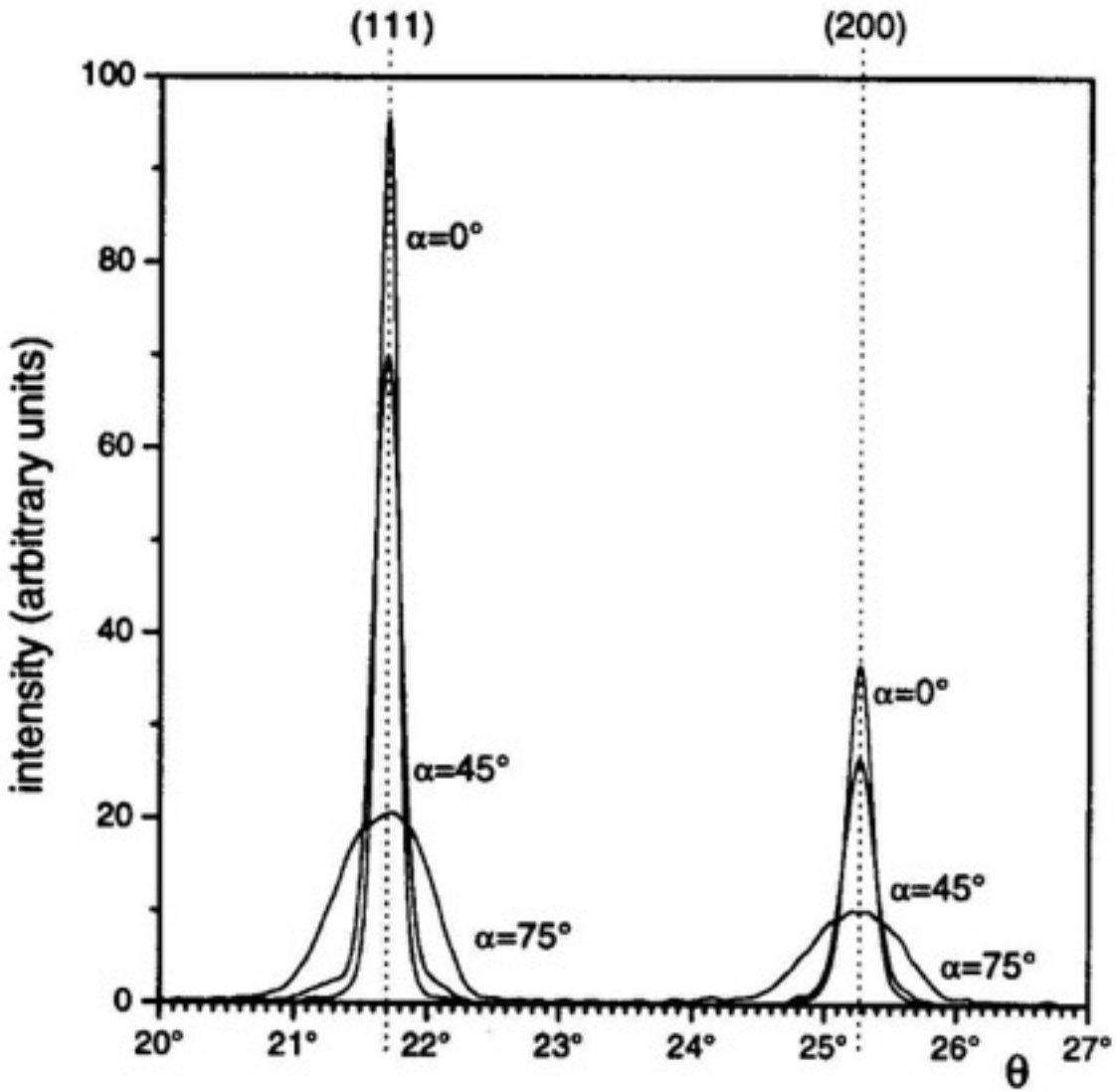

Visualizing of Defocusing Error

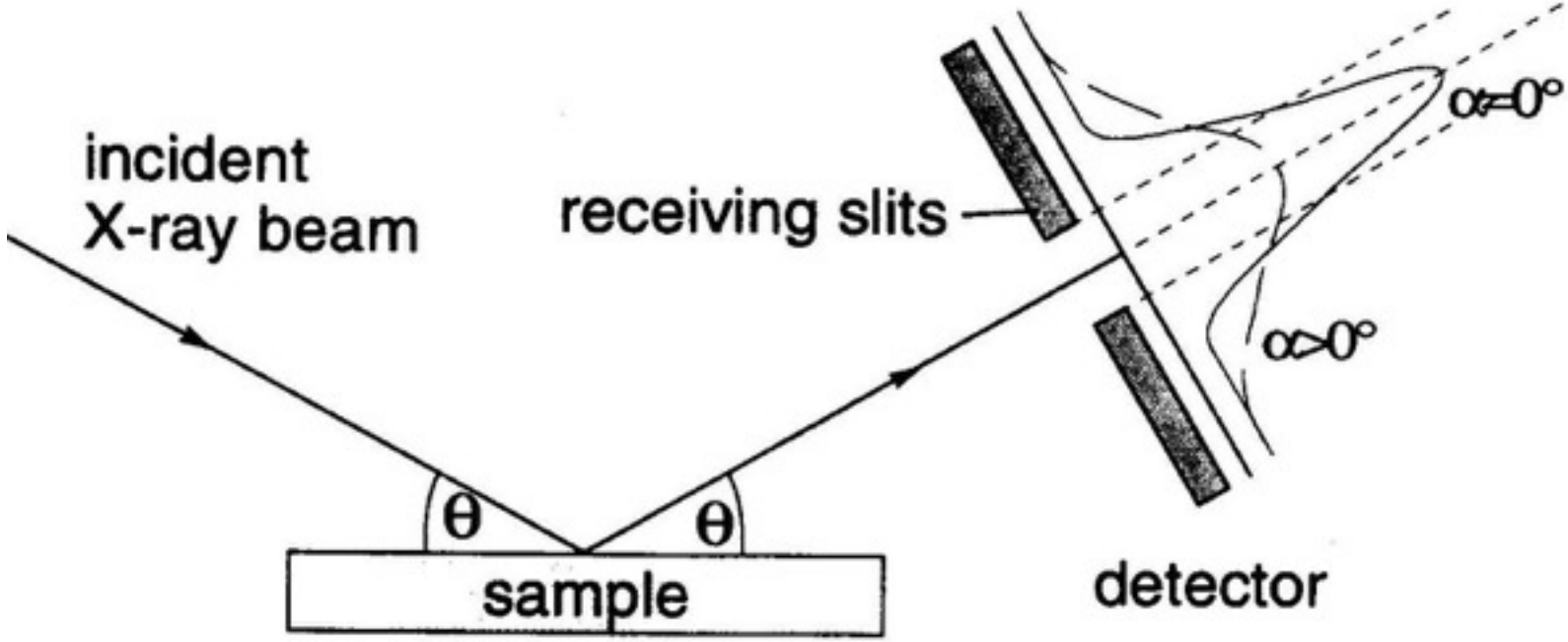

Pole figure scanning mode: step scan

Old goniometer

New goniometer

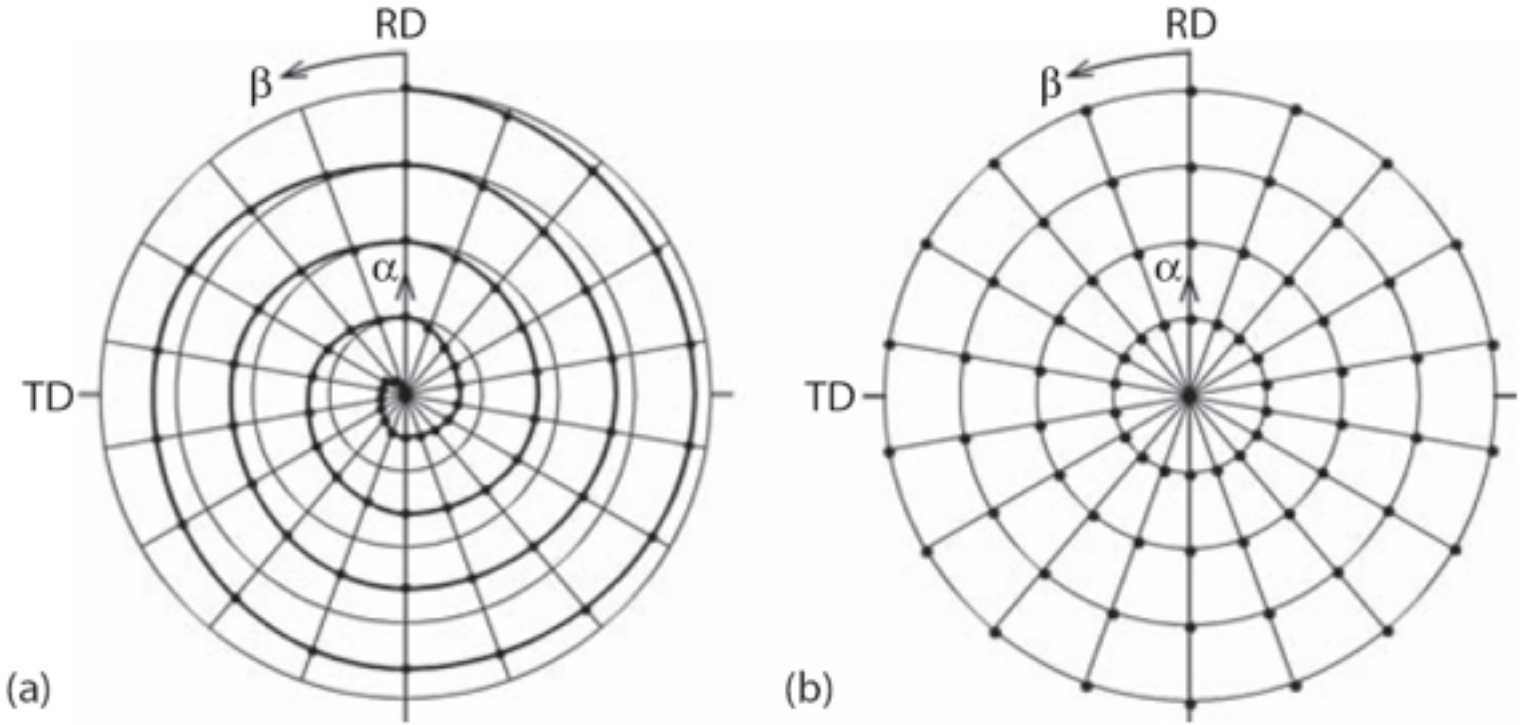

FIGURE 4.12
(a) Spiral and (b) circular, equal-angle scanning grids for pole figure measurements (note that for clarity both scanning schemes are shown in steps of 20°).

Pole figure scanning mode: continuous scan

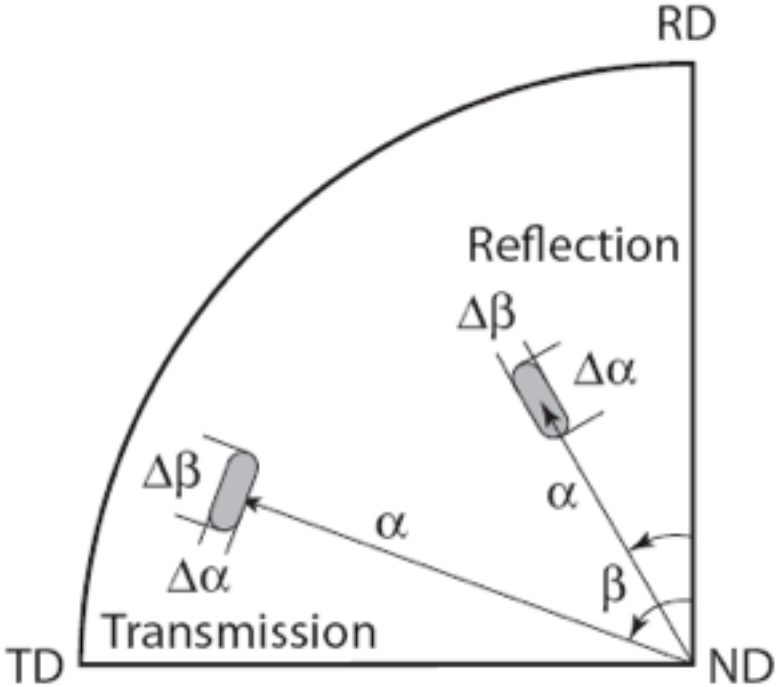

FIGURE 4.13
Shape of the pole figure window for reflection and transmission geometry.

Pole figure scanning mode: Equal area scanning

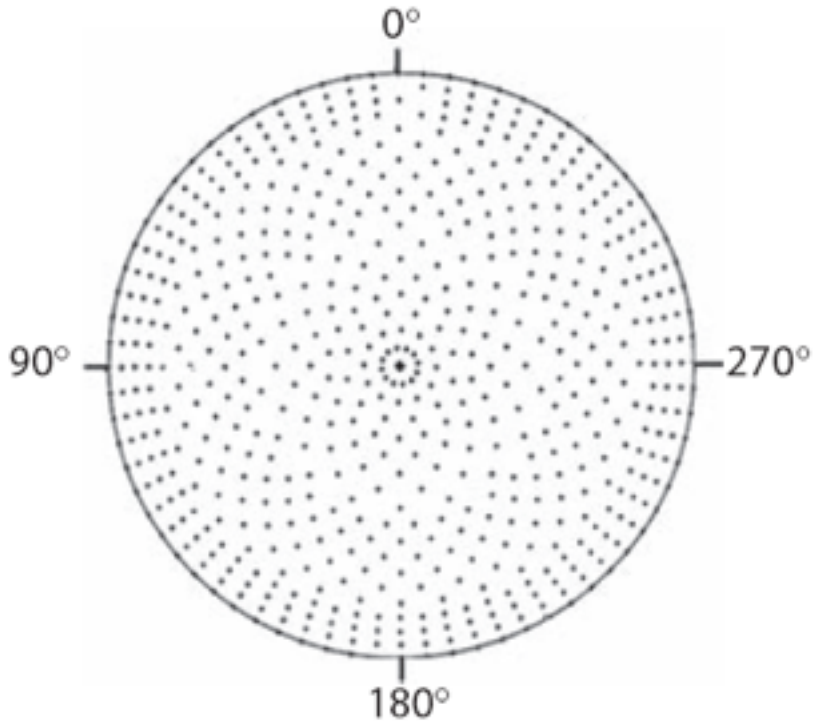

FIGURE 4.14
Equal area scanning grid for pole figure measurements. (Adapted from Brokmeier, H.-G., *Textures Microstruct.*, 10, 325, 1989.)

X-Ray detector: Geiger counters

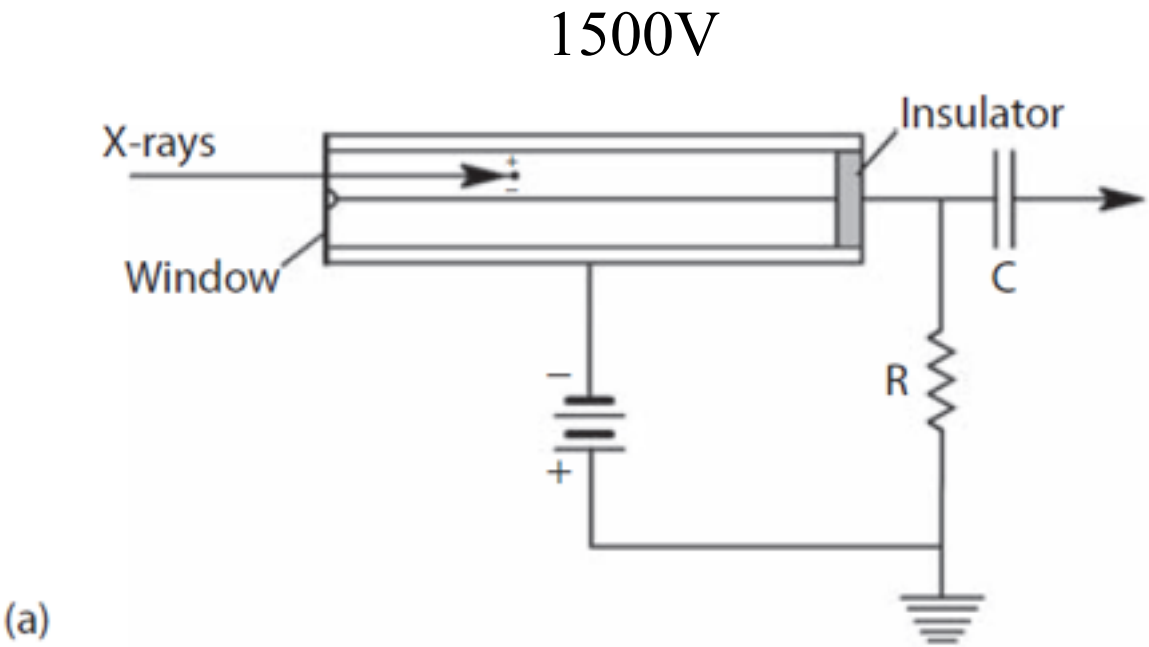

X-Ray detector: Proportional counters

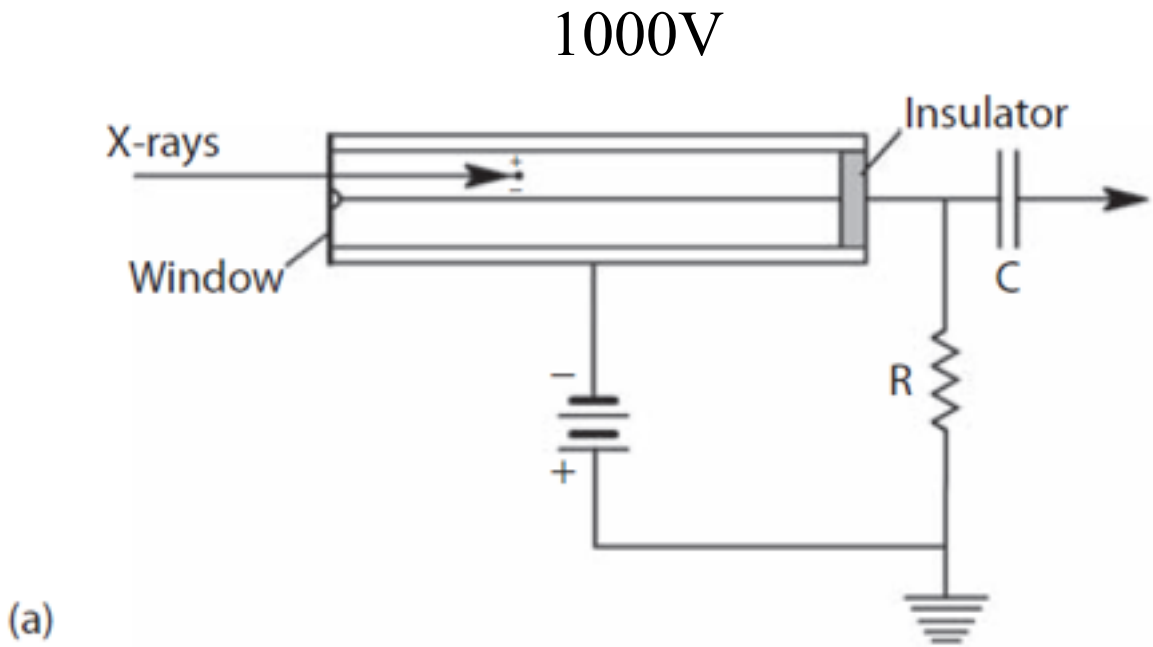

X-Ray detector: Scintillation counters

- Geiger counters
- Scin
- Prop
- Sem

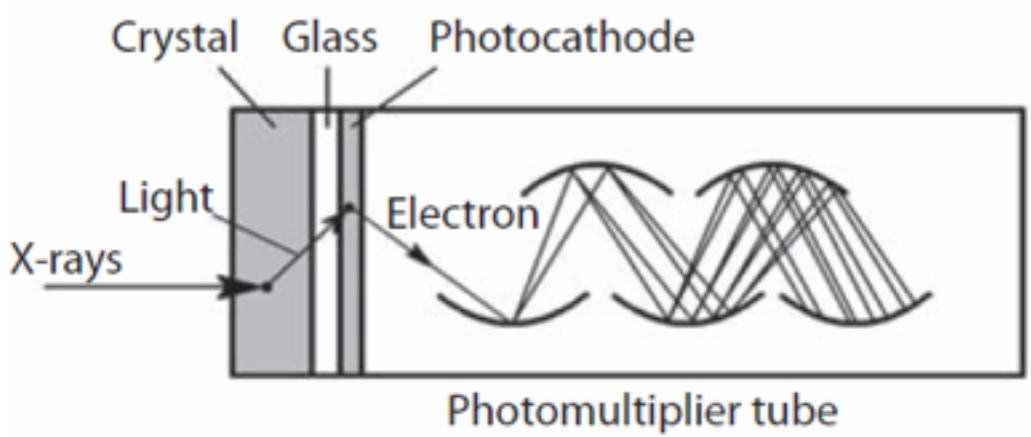

(b)

X-Ray detector: Semiconductor counters

- Geiger counters
- Scintillation counters
- Proportional counters
- Semic

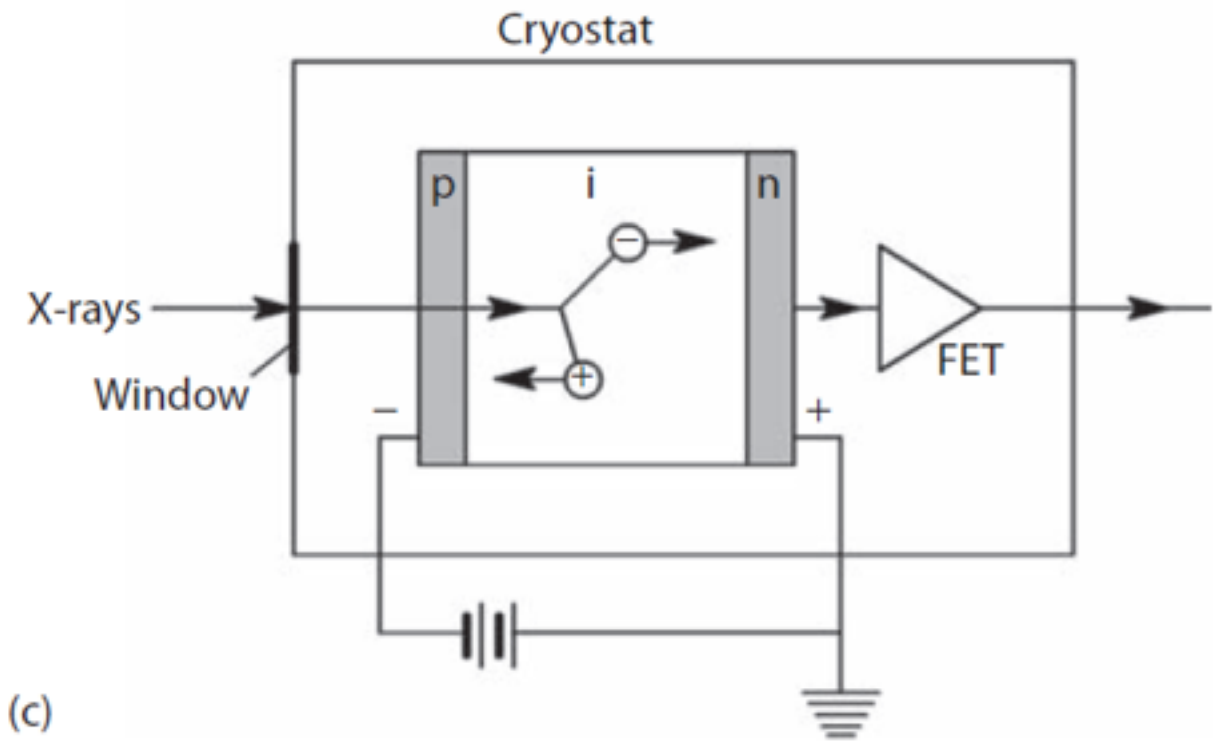

Principle of 1D-PSD detector

$$\frac{U_l}{U_r} = \frac{x}{l - x}$$

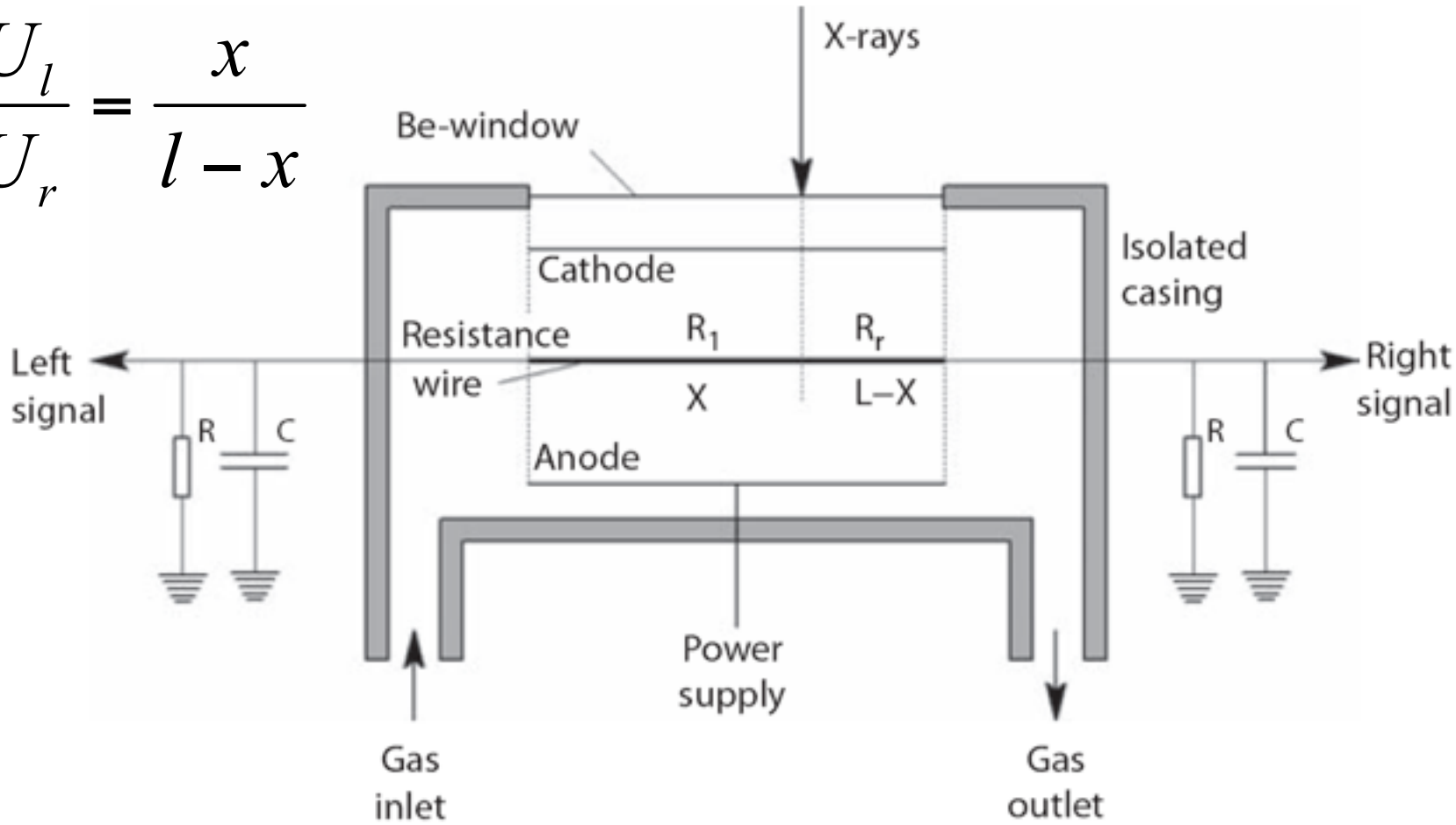

(a)

Pole figure measurement using 1D detector

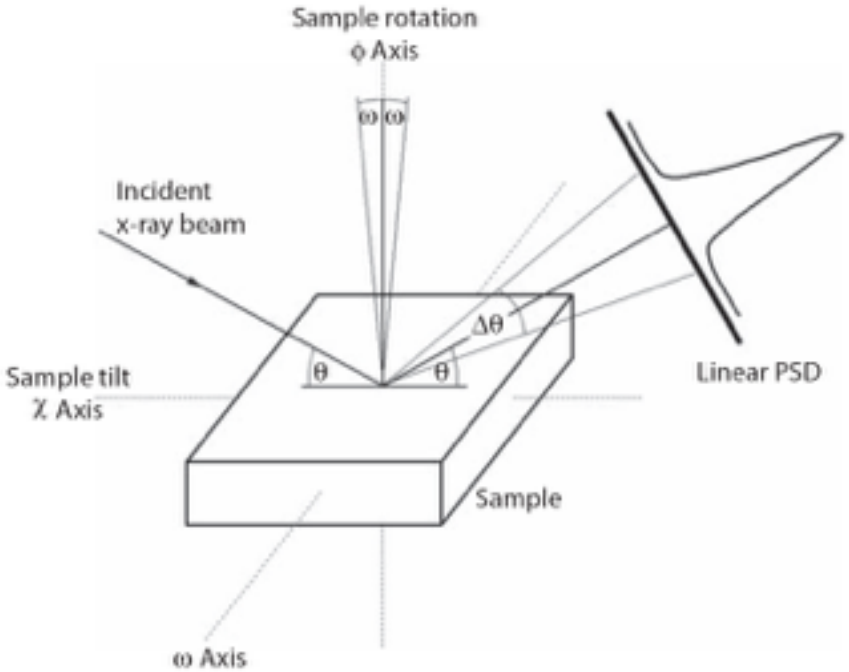

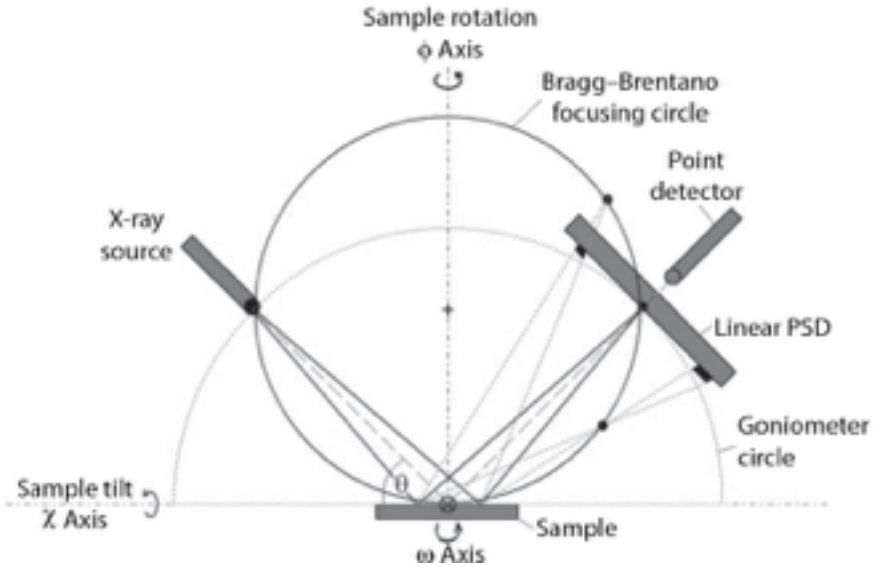

Pole figure measurement using area detector

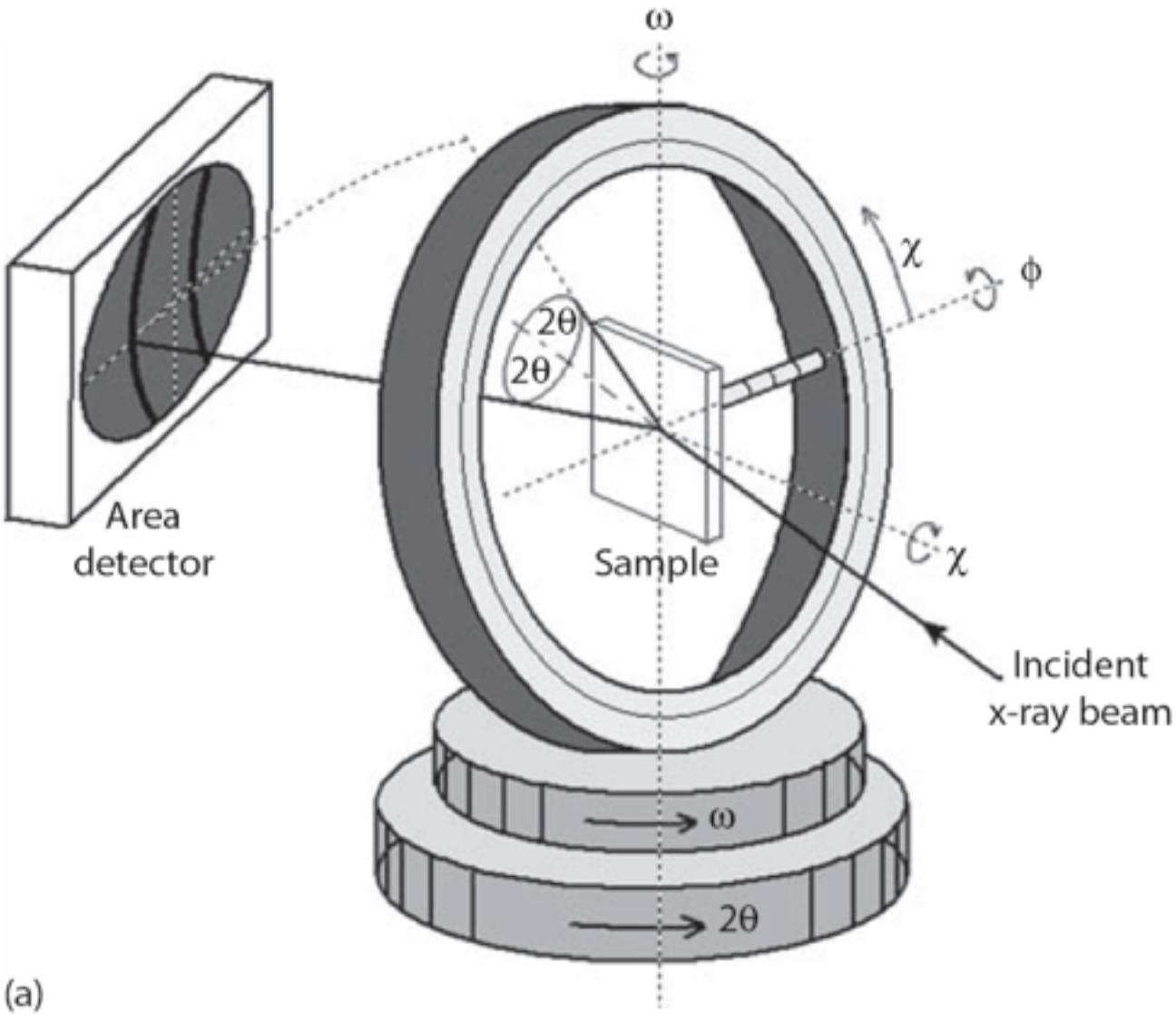

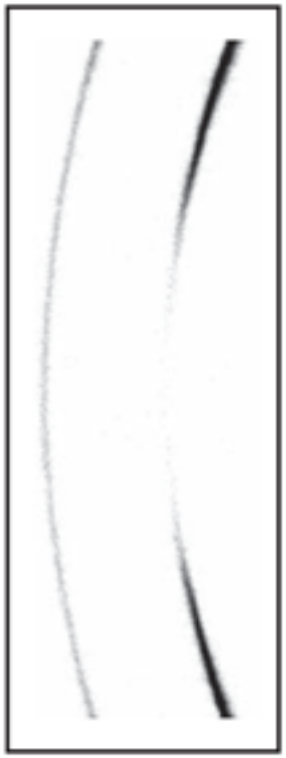

Pole figure coverage with two β scans

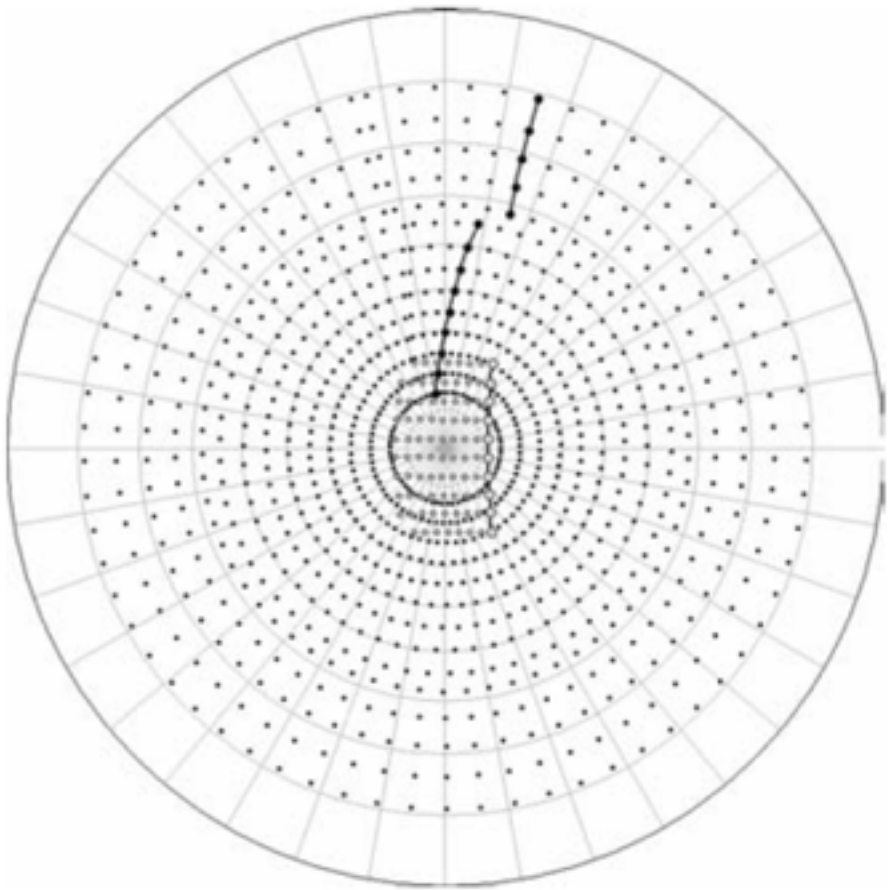

FIGURE 4.17
Pole figure coverage with two β scans (rotations) for $\alpha = 40°$ and $80°$ (black symbols) and one ω scan at $\alpha = \beta = 0°$ (gray symbols). In this example, the diffraction angle was $2\theta = 45°$, enabling simultaneous analysis of {111} and {200} pole figures in an aluminum sample.

Angular and energy-dispersive diffractions

A: energy-dispersive diffraction

$$E = \frac{hc}{2\sin\theta} \cdot \frac{1}{d_{hkl}}$$

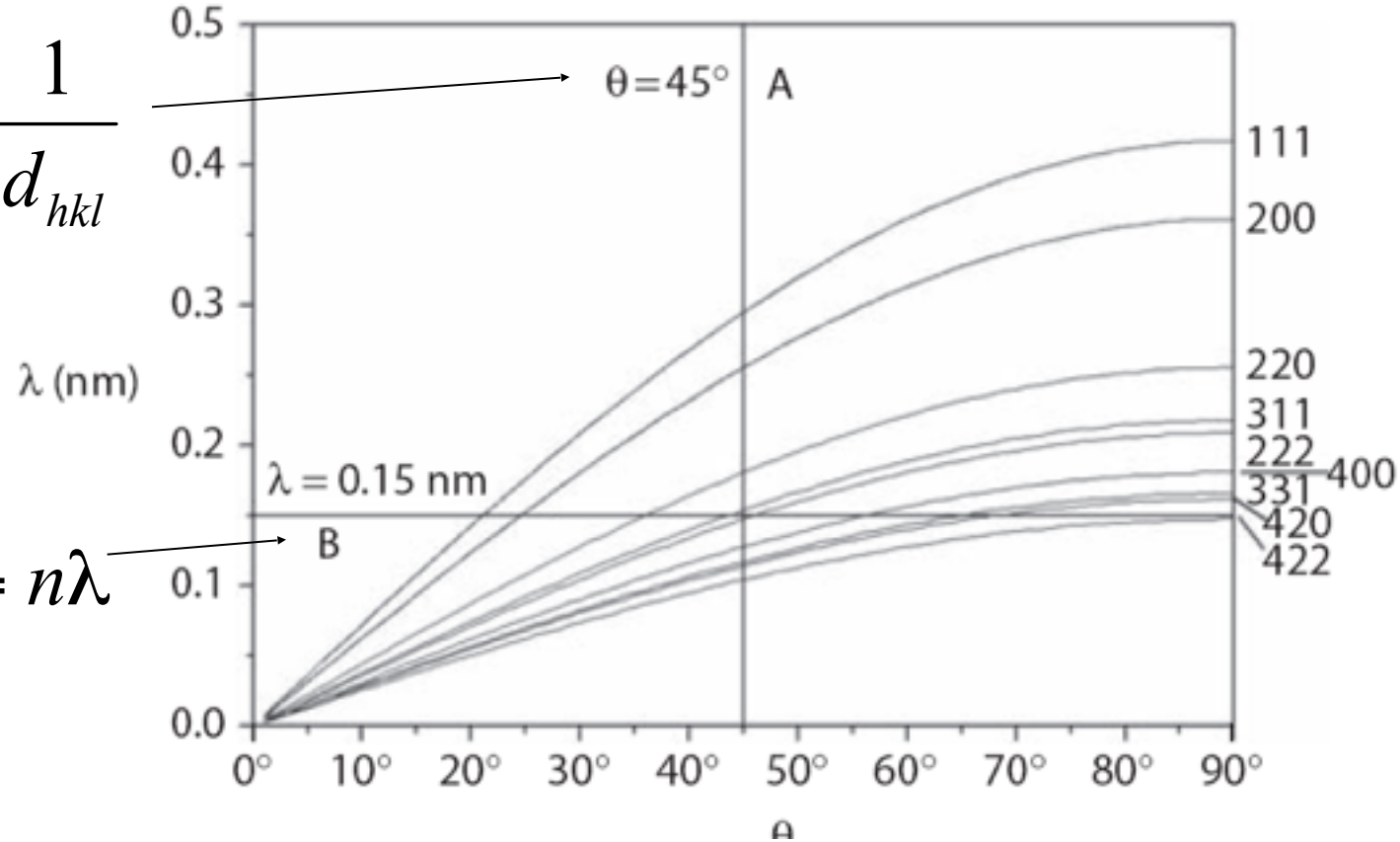

$$2d_{hkl}\sin\theta = n\lambda$$

B: angular-dispersive diffraction

Energy-dispersive diffraction spectrum

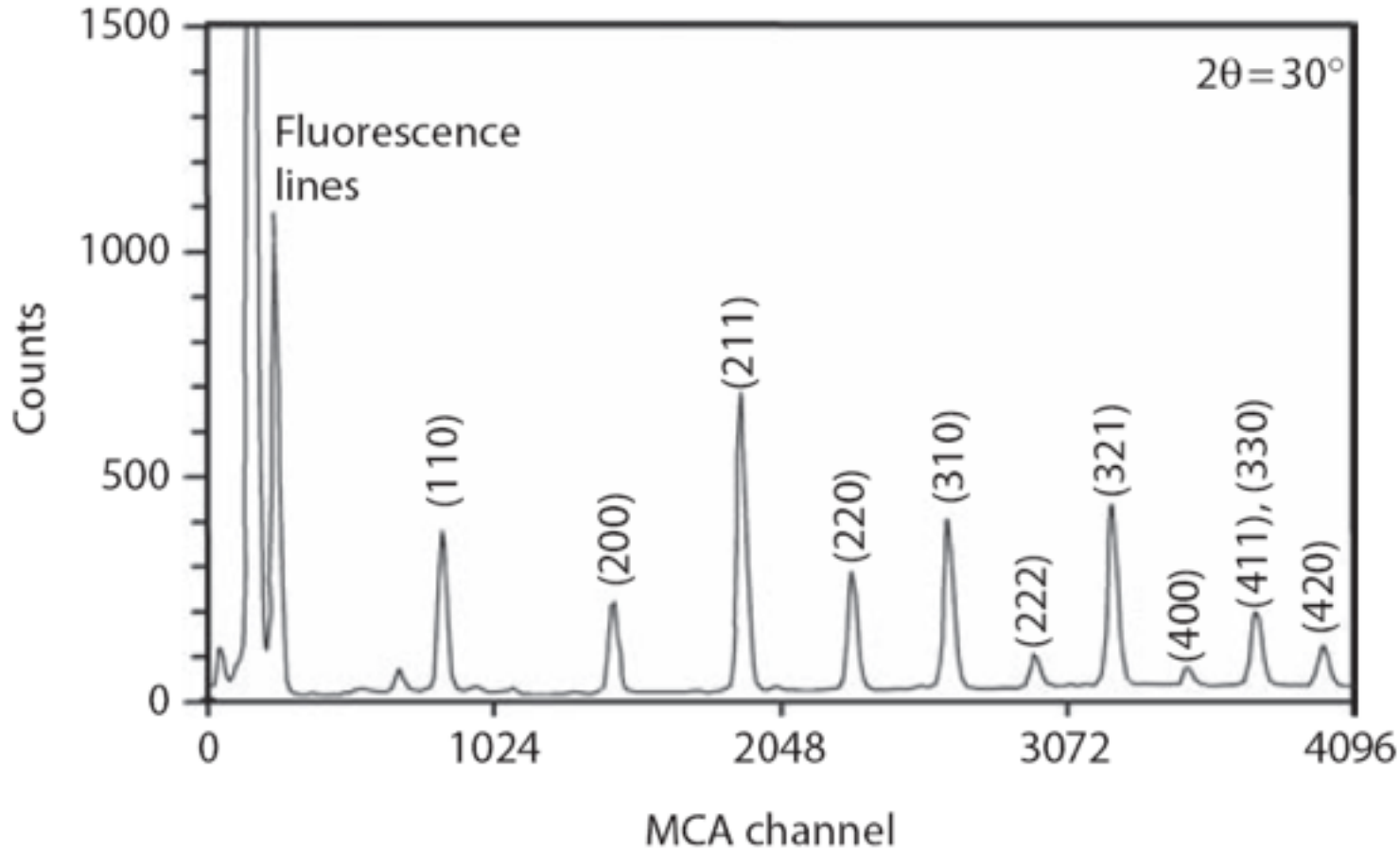

Diffraction time: 200s and

2 θ =30°, CrKα

$$E = h\nu = h\frac{c}{\lambda} = \frac{hc}{2\sin\theta}\cdot\frac{1}{d_{hkl}}$$

Intensity Distributions of Error

- **Intensity to pole density conversions include:**
  - Absorption corrections (necessary for tilts >70 degrees)
  - Defocusing corrections
  - Background corrections
  - Variable diffracting volume (especially for thin films)
- **Corrections in pole figure space:**
  - Sample misalignment
  - Parallax errors (detector space)
  - Interpolation in pole figure space
  - Pole figure normalization
- **Goniometer misalignment errors are generally not correctable (e.g. peak shifts with tilt, etc.)**
- **Individual pole figures and sets of pole figures must be self-consistent**

Background Error-cont.

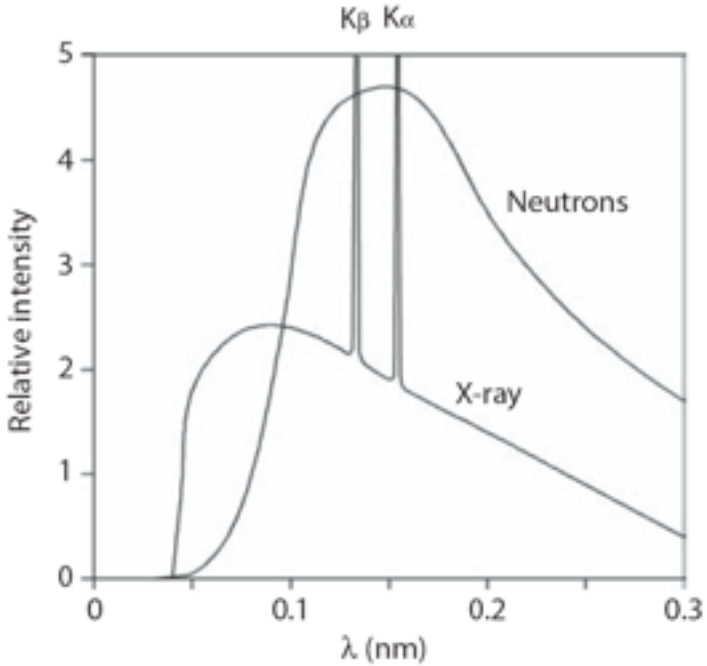

To prevent other wavelength of the continuous spectrum:
with K_β filter, whose absorption edge lies between K_α and K_β
By using single crystal monochromataor

$$I_{corr} = I_{mean}(\alpha, \beta) - BG(\alpha)$$

Background Error-cont.

TABLE 4.1

Characteristics of Various X-Ray Tubes and Appropriate Filters

	Wavelength (nm)		Kβ Filter			
Anode Material	Kα	Kβ	Material	Edge Wavelength (nm)	Thickness for Kβ/Kα = 1/500 (μm)	Loss in Kα (%)
Cr	0.22909	0.20848	V	0.22690	17	51
Fe	0.19373	0.17565	Mn	0.18964	18	53
Co	0.17902	0.16208	Fe	0.17433	19	54
Cu	0.15418	0.13922	Ni	0.14880	23	60
Mo	0.07107	0.06323	Zr	0.06888	120	71
Ag	0.05609	0.04970	Rh	0.05338	92	73
			Pd	0.05092	90	74

Source: Data taken from Hahn, T. (Ed.), in *International Tables for Crystallography Vol. A*, Springer-Verlag, Dordrecht, the Netherlands, 2005.

Correlation of background intensity

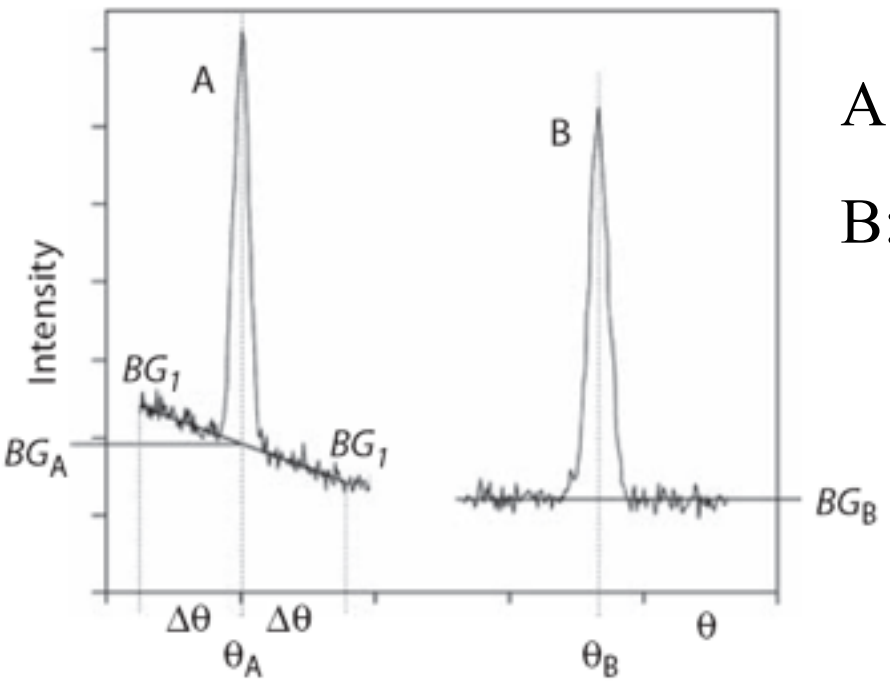

A: background in dependence of θ

B: background is independent of θ

$$I_{corr} = I_{mean}(\alpha, \beta) - BG(\alpha)$$

- Incoherent scatting
- Fluorescence
- Interaction of X-ray beam with collimator, beamstop and air
- Other wavelength of the continuous spectrum
- Electronic noise

Absorption Error

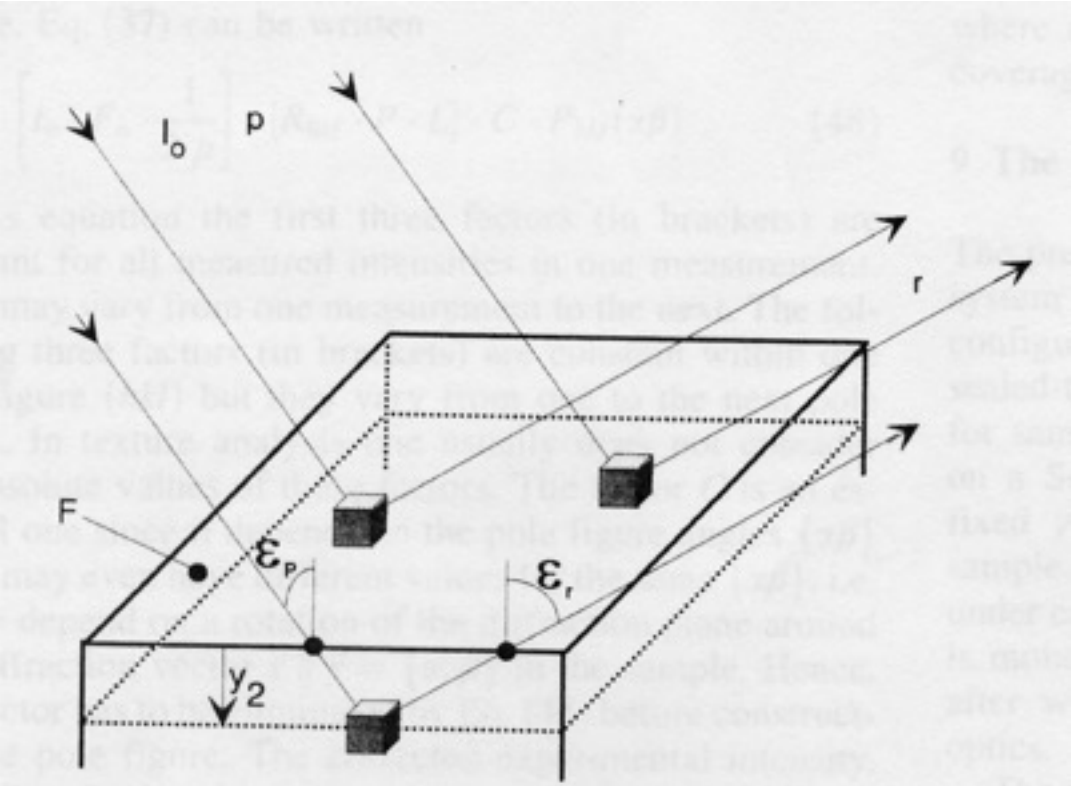

Fig. 13. Reflection of X-rays in volume elements at y_2 below the sample surface.

Another important aspect of absorption is the depth of X-ray penetration

Penetration volume

Intensity

Absorption Error

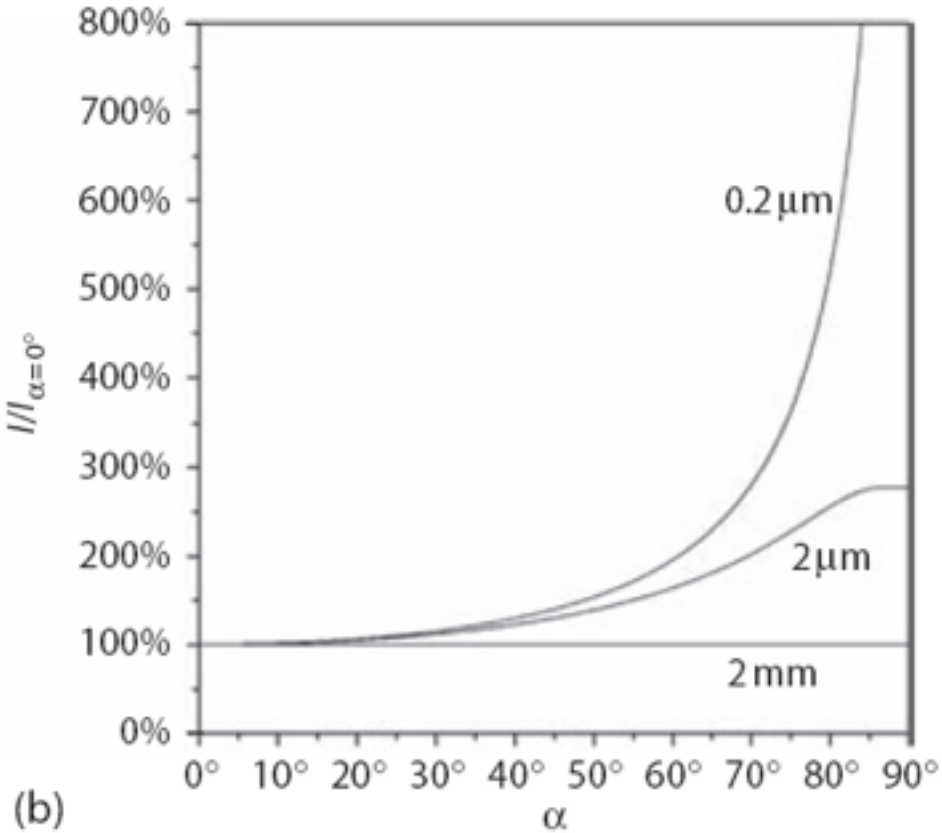

$$I_{\exp}^{\text{int}}(\alpha,\beta) = I_{cor}^{\text{int}}(\alpha,\beta)\cdot C$$

$$I_{cor}^{\text{int}}(\alpha,\beta) = \frac{I_{\exp}^{\text{int}}(\alpha,\beta)}{C}$$

Absorption correlation factor

Geometry Distortion

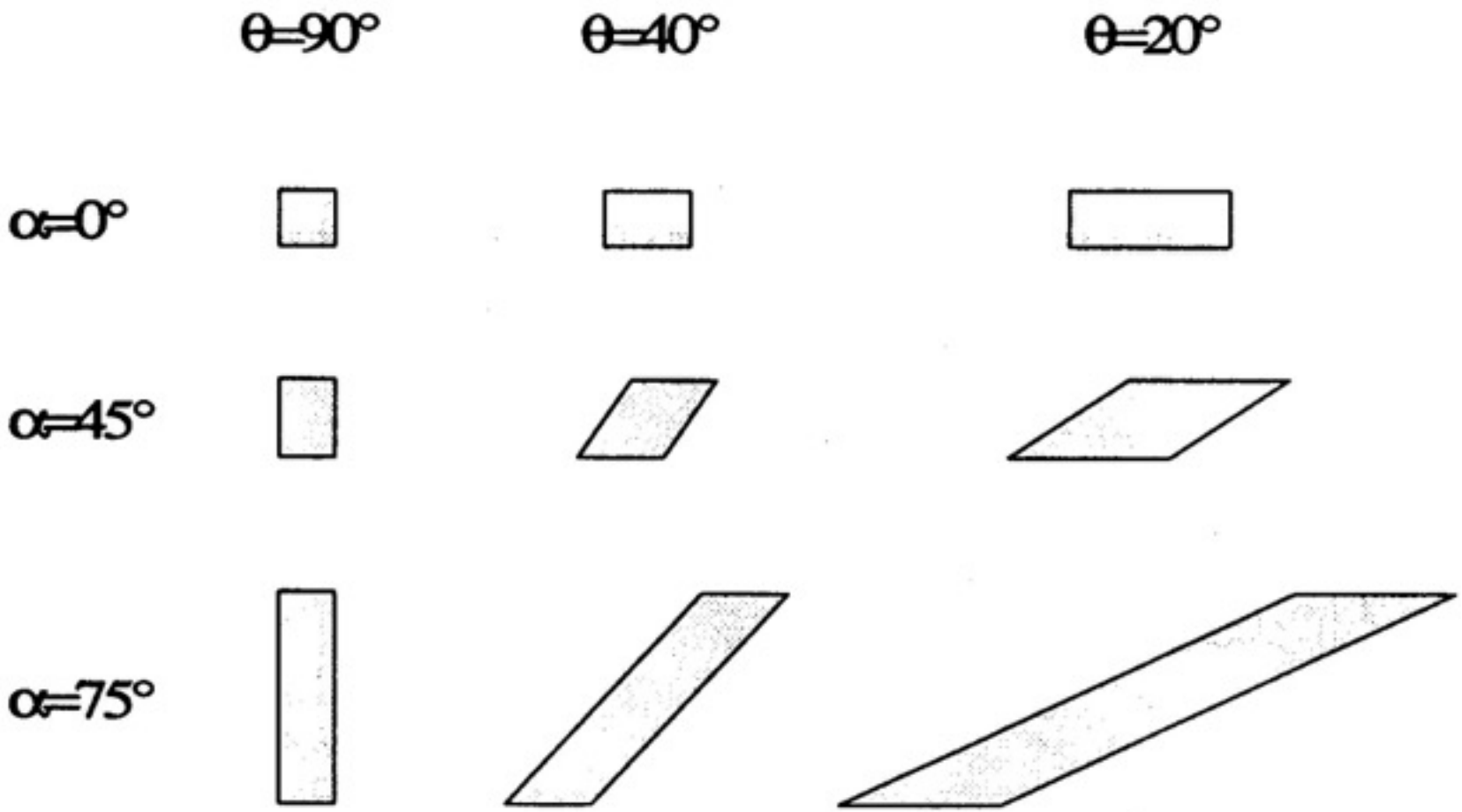

Peak Broadening

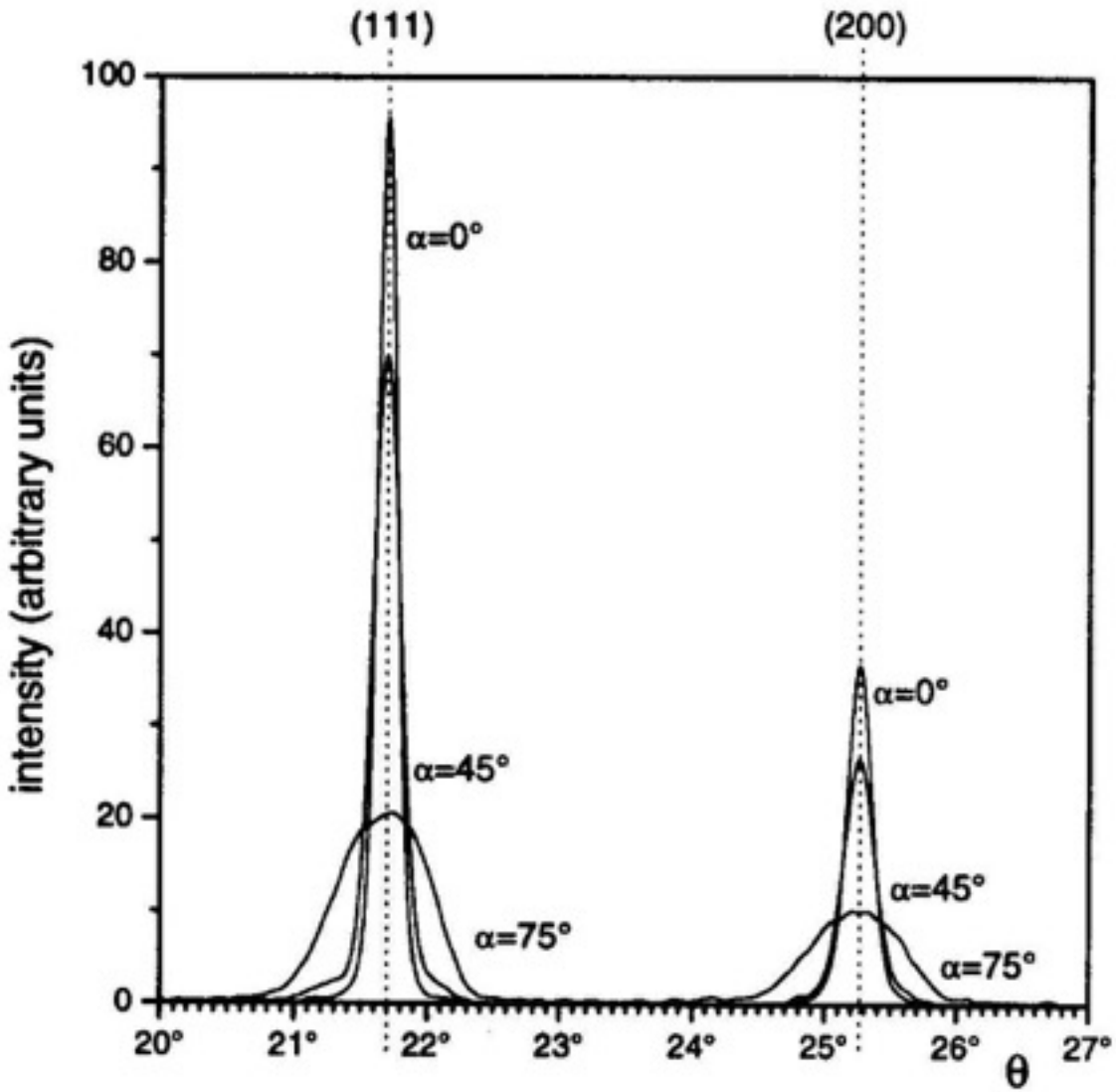

Visualizing of Defocusing Error

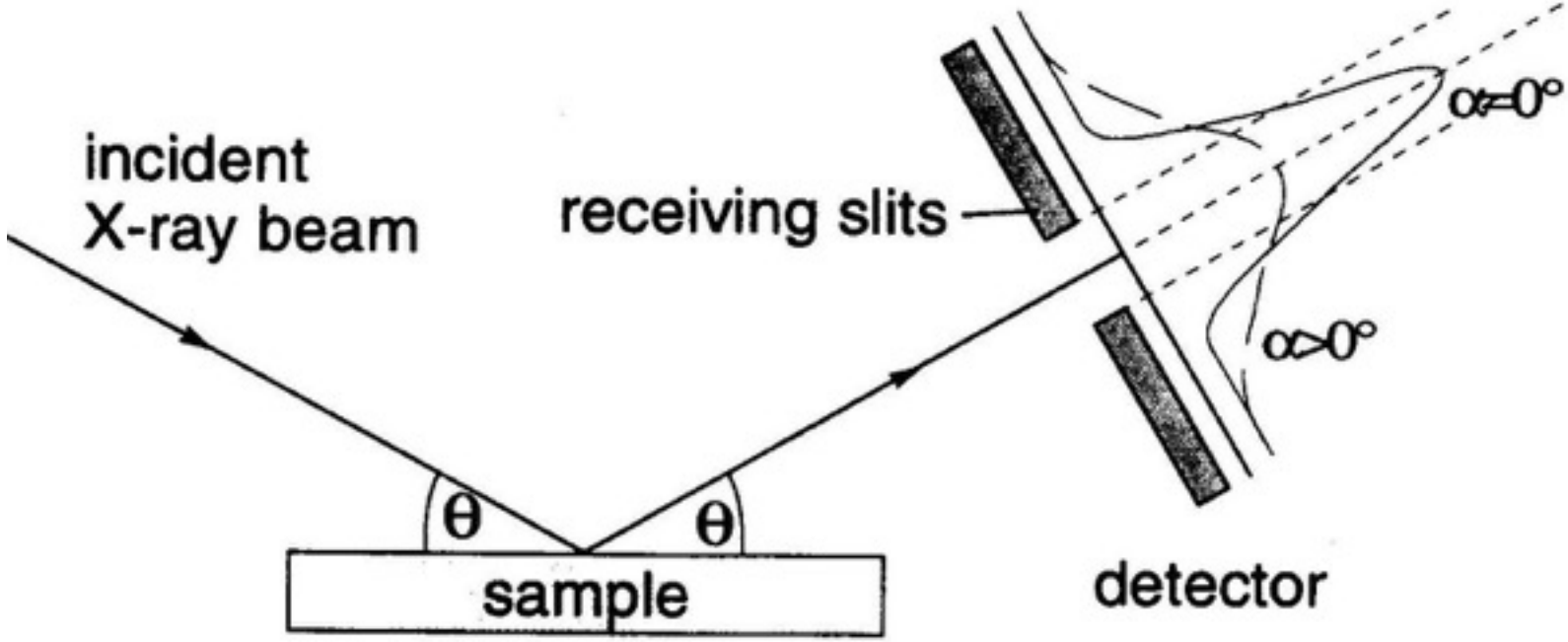

Defocusing Error

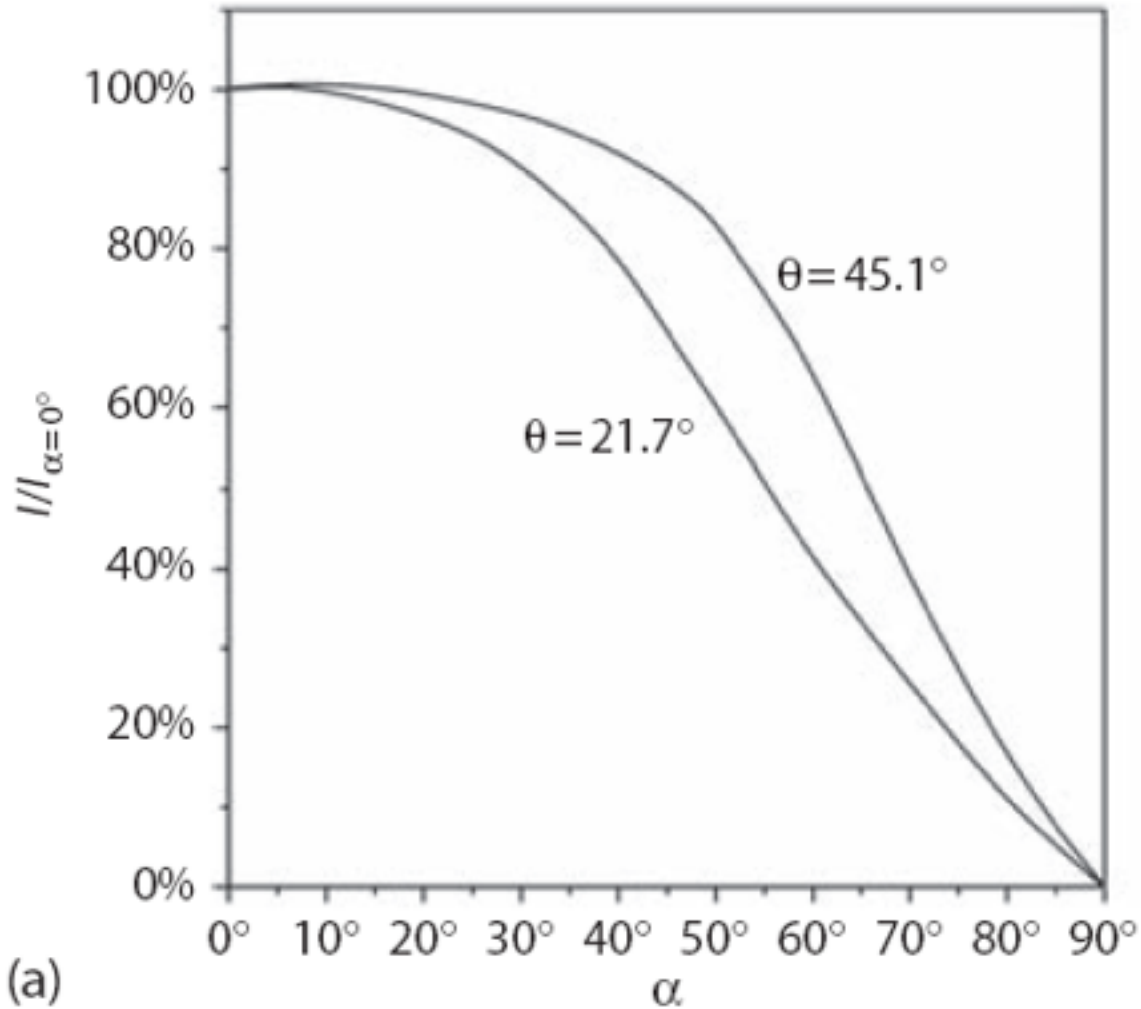

Defocusing Error

As inclination (Ψ) of the sample increases, the peaks in the diffraction pattern are broadened. Thus the measured intensities can be corrected by measuring a defocusing scan on a texture free sample (preferably of the same composition). If such a sample does not exist, defocusing corrections can be estimated from the stored data.

$$I_{corr} = \frac{I_{mean}(\alpha, \beta) - BG(\alpha)}{U(\alpha)}$$

Example of defocusing Error

Values for correcting data

Tilt Angles

```
demo     (from Cu1S40, smoothed a bit: UFK)
111
```

0	1000.00
5	999.
10	999.
15	999.
20	999.
25	999.
30	999.
35	999.
40	999.
45	999.
50	999.
55	982.94
60	939.04
65	870.59
70	759.37
75	650.83
80	505.65
85	344.92
90	163.37
	2.19

At each tilt angle, the data is multiplied by 1000/ value

Values for correcting background

Tilt Angles

0	100.00
5	100.00
10	100.00
15	100.00
20	100.00
25	100.00
30	100.00
35	100.00
40	100.00
45	100.00
50	99.00
55	96.00
60	92.00
65	83.00
70	72.00
75	54.00
80	32.00
85	13.00
90	.00

Normalization (Counting Statistics)

Normalization is the operation that ensures that "random" is equivalent to an intensity of one.

Normalization factor:

$$N = \frac{\int_i I_{corr}(\alpha,\beta)\sin\alpha_i}{\int_i \sin\alpha_i}$$

Normalization of inentsity:

$$I_{norm}(\alpha,\beta) = \frac{1}{N} \cdot I_{corr}(\alpha,\beta)$$

Inverse pole figure

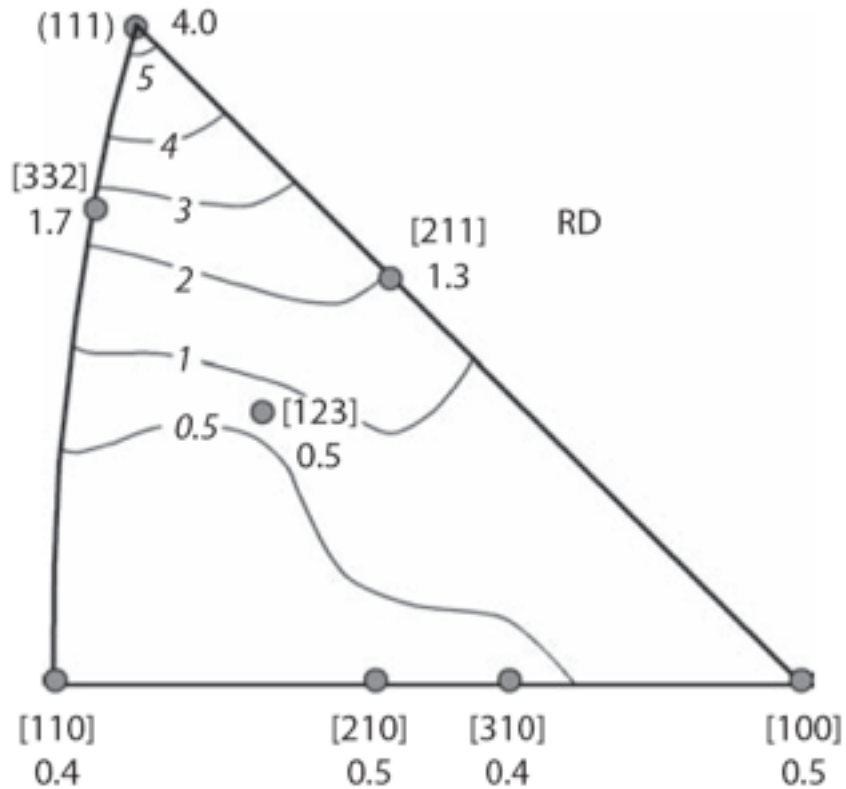

FIGURE 4.22
Inverse pole figure of the sheet normal direction ND obtained from a commercially produced stabilized steel sheet in the temper-rolled condition. Measured points—inverse pole figure measured as described in the text; intensity lines—inverse pole figure recalculated from the three-dimensional ODF. (Adapted from Bunge, H.-J. and Roberts, W.T., *J. Appl. Crystallogr.*, 2, 116, 1969.)

Neutron diffraction methods

The first texture measurements using neutron diffraction were performed in 1953 at Chalk River Nat. Lab.

This technique was further developed by Tobish and coworkers (1968, 1969, 1976). More sophisticated methods like time-of-flight (TOF) measurements off additional advantages over x-ray diffraction techniques.

Wavelength spectrum of neutron source

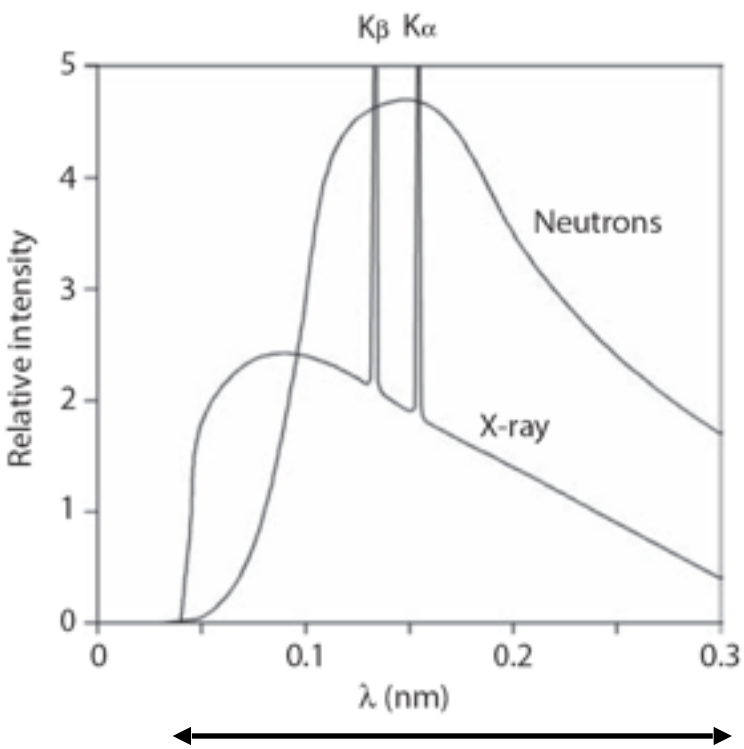

0.05nm 0.3nm

The principle of pole figure analysis by neutron diffraction is equivalent to x-ray pole figure measurements.

Copper (111) or graphite (0002) monochromator crystals are used.

Copper x-ray tube

Principle of pole figure measurement

The neutron detector is set to Bragg angle 2 θ for {hkl} plane.
The pole intensities of this plane are scanned by rotating two φ and χ to cover the entire orientation range.

Advantages:

1. negligible absorption
2. several centimeter penetration depth
3. no intensity correction
4. in situ investigations during heating, cooling, and straining

Drawback:

Neutron diffraction is that the intensity is much lower than that of x-ray. 6- 48h for a pole figure by neutron, compared to 30 min for x-ray.

Time-of-flight (TOF) diffraction measurement

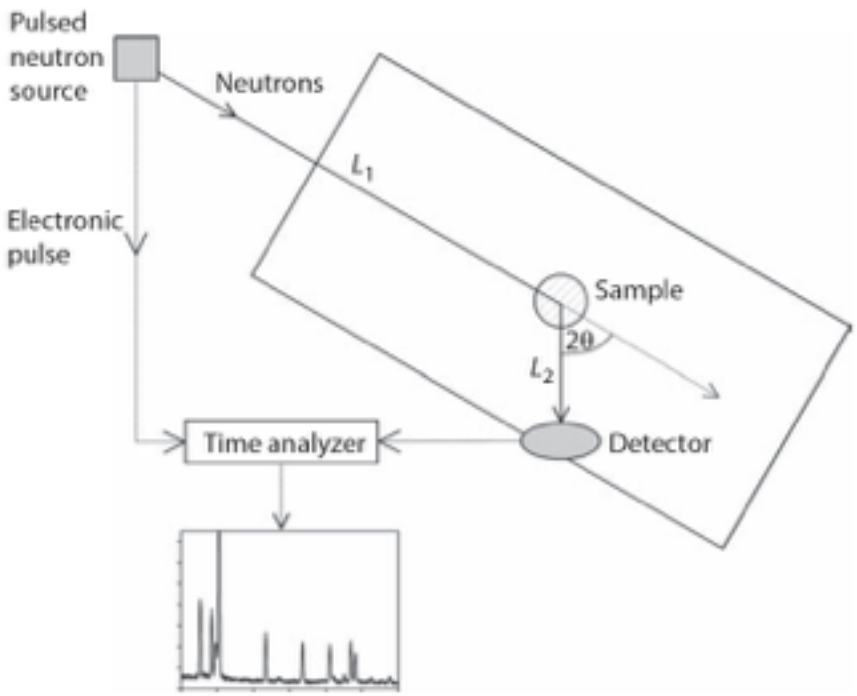

As no energy-sensitive detectors for neutrons are available, therefore, the flight time of neutrons is used to determine their energy or wavelength. It is called time-of-flight (TOF).

$$E = \tfrac{1}{2} m_N v_N^2 = \frac{h^2}{2\lambda^2 m_N}$$

FIGURE 4.24
Schematic arrangement to perform TOF measurements. The total flight time T of the neutrons is determined by their velocity and the length L_1 between source and sample and L_2 between sample and detector.

Time-of-flight (TOF) diffraction measurement

The energy spectrum for neutrons is between 10^{-3} and 10 eV (corresponding to λ = 0.5 and 0.01nm).

The velocities are in the range of 10^3 to 4×10^4 ms^{-1}.

$$t_{TOF} = \frac{(L_1 + L_2)}{v_N} = \frac{(L_1 + L_2)}{(2E/m_N)^{1/2}} = \frac{(L_1 + L_2) \cdot h}{\lambda m_N}$$

A combination of PSDs and TOF would speed up pole figure measurements and it has been realized at the Intesne Pulsed Neutron Source at Argonne National Laboratory.

Neutron time-of-flight diffractometer HIPPO

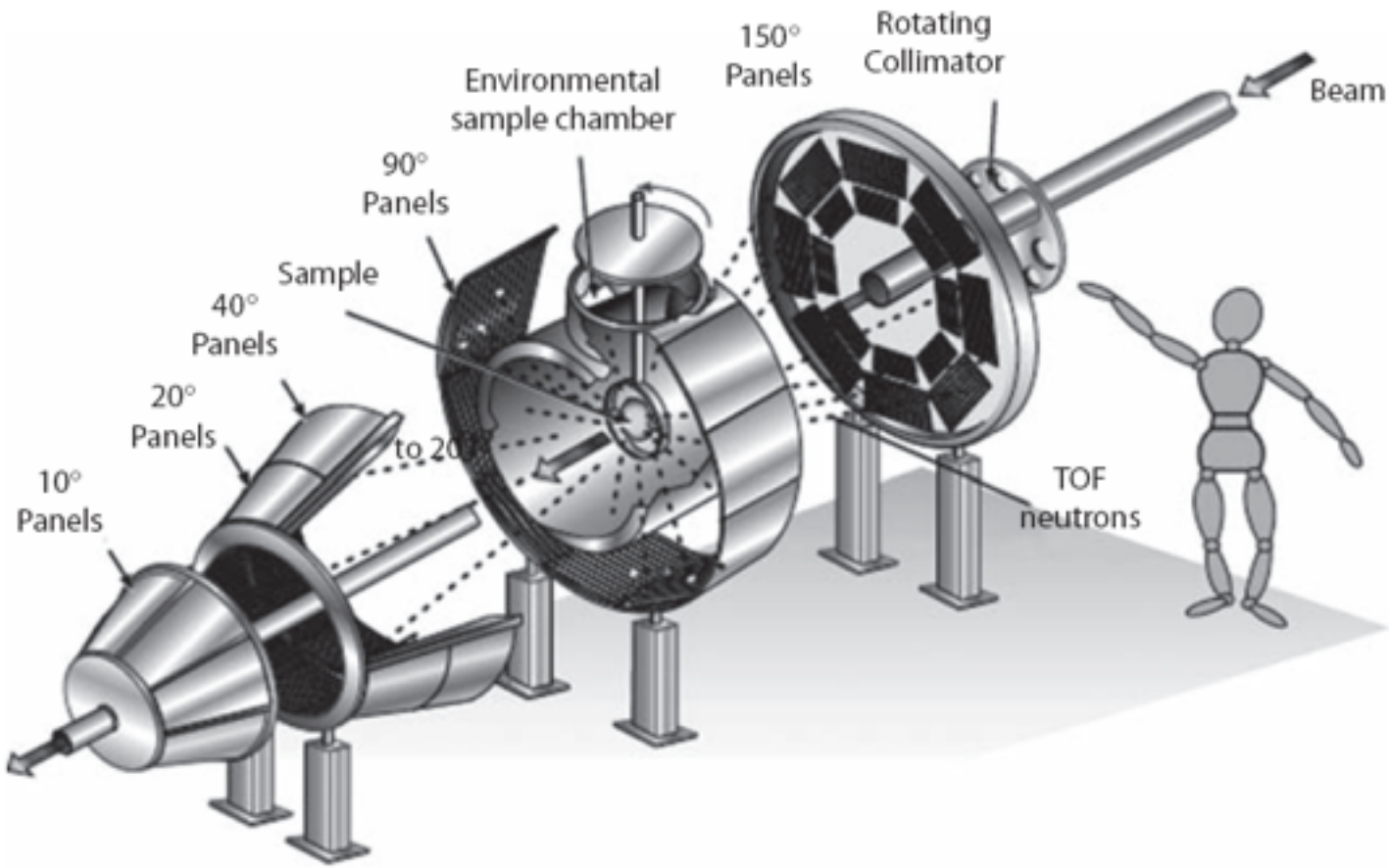

FIGURE 4.25
Schematic view of the neutron time-of-flight diffractometer HIPPO with five banks of detector panels arranged on rings of constant diffraction angle. The sample is located in a sample chamber. For scale a sketch of a fairly large person is added; the distance from the 150° panels to the 10° panels is 3 m. (Courtesy of S. Vogel.)

Low symmetry materials and multiphase materials

Problems:

1. Problems with peak separation caused by peak-rich diffraction spectra in both mutliphase and low-symmetry materials

2. Volume fraction of the various phases in mutliphase materials

3. Anisotropic absorption of the reflected x-rays in mutliphase materials

Neutron diffraction and EBSD don’t have such above problems.

Low symmetry materials and multiphase materials

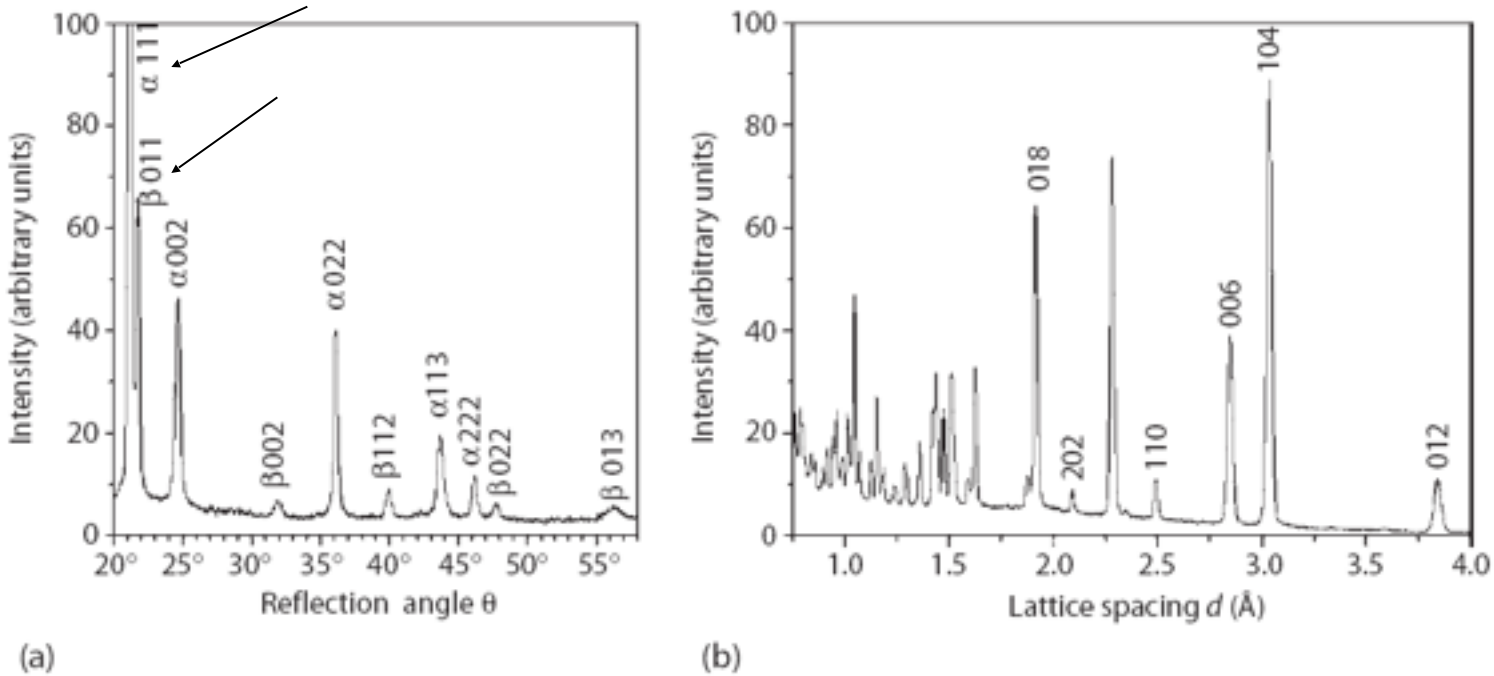

FIGURE 4.26
Examples of line-rich diffraction spectra. (a) Two-phase brass (Cu–40%Zn, x-ray θ/2θ spectrum). (From Engler, O. and Juul Jensen, D., *Scr. Mater.*, 30, 25, 1994. With permission.) (b) Calcite (neutron TOF spectrum.) (Data from Lutterotti, L., Matthies, S., Wenk, H.-R., Schultz, A.J., and Richardson, Jr. J.W., *J. Appl. Phys.*, 81, 594, 1997.)

Partial coincidence of reflection peaks: the difference between {111} and {011} is 0.5°.

X

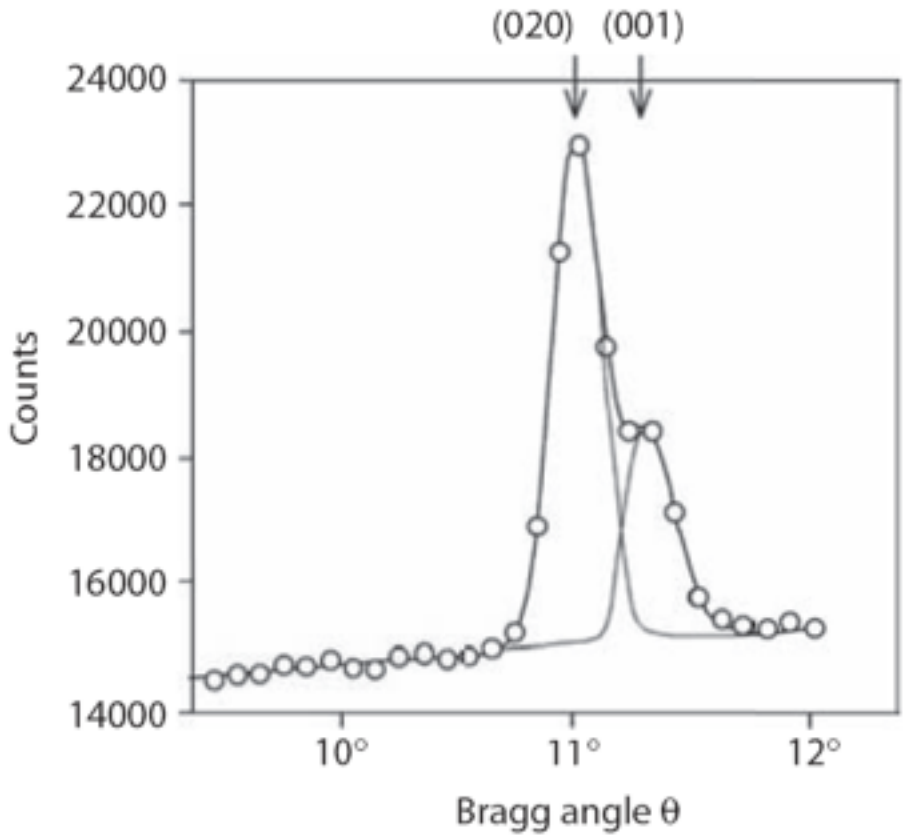

FIGURE 4.27
Separation of two partially overlapping feldspar diffraction peaks recorded by a linear PSD. (Adapted from Brokmeier, H.-G., *Textures Microstruct.*, 10, 325, 1989.)

Low symmetry materials

Partial coincidence of reflection peaks: the difference between {111} α and {011} β is 0.5°

Completely overlap of reflection peaks: the same lattice spacing of lattice planes {330} and {411}; for α/γ duplex steel the {111} peak of fcc and the {011} peak of bcc are overlap

The Rietveld texture analysis (RTA) is expected to improve quantitative texture analysis of low-symmetry compounds and multiphase materials.

Mutliphase materials

Problems:

1. It is difficult to determine properly pole figure of phases with small volume fractions. In general, 5% vol% can be estimated to the lower limit for texture analysis by x-ray diffraction.

2. In deformed materials the various phases are highly aligned along deformation direction. Difference in the absorption of x-ray in the diffraction phases can cause errors in x-ray texture measurements.

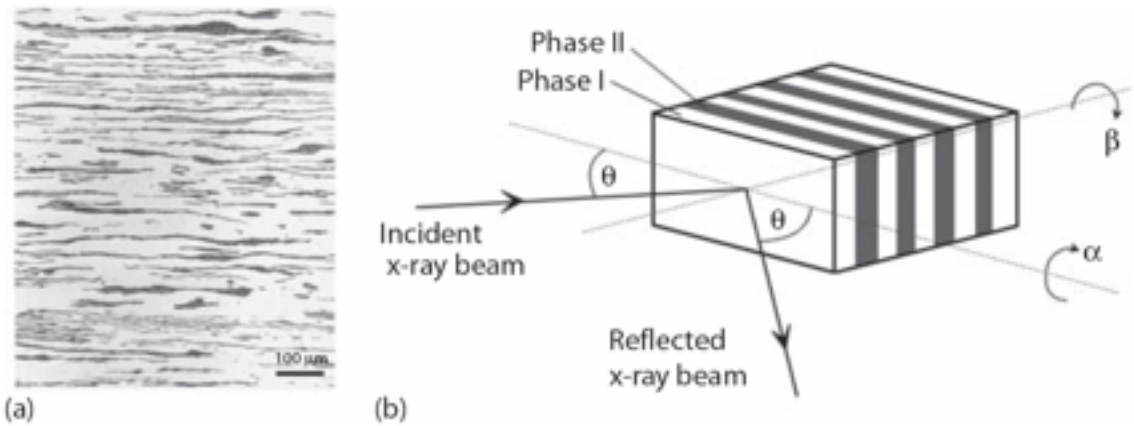

FIGURE 4.28
(a) Microstructure of cold-rolled two-phase Cu–40%Zn illustrating the alignment of the phases with deformation. (b) Schematic representation of the reflection of x-rays during pole figure measurements, illustrating the occurrence of anisotropic absorption in layered two-phase structures.

Sample preparation for neutron measurements

The spherical sample method was used for neutron texture analysis, because no absorption in this geometry is necessary and large penetration depth.

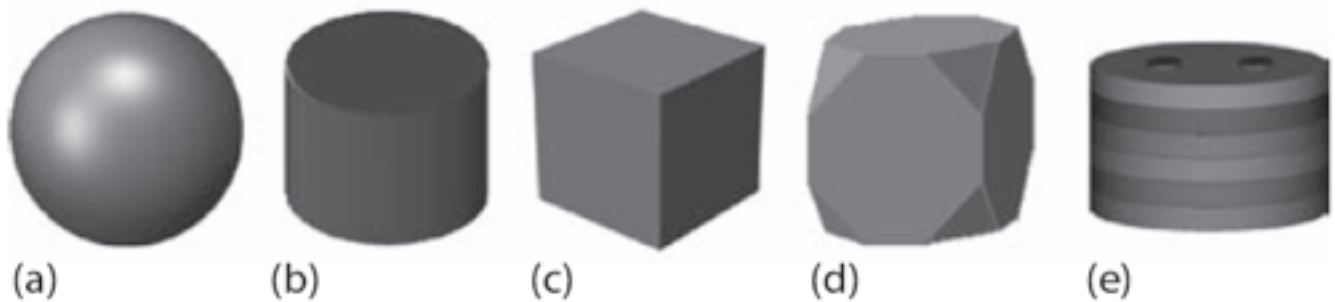

FIGURE 4.29
Samples for texture analysis through neutron diffraction. (a) Spherical sample; (b) cylindrical sample; (c) cubic sample; (d) cubic sample with rounded edges; (e) cylindrical composite sample produced by stacking several disks cut from a thin sheet.

Sample preparation for x-ray measurements

Texture measurements in transmission geometry require thin sample with thickness below 100 μm.

To obtain wire textures, a bundle of parallel wires is mounted and the cross section of a bundle of wires can be conducted for texture measurements.

Texture measurements in reflection geometry require sample geometry with rectangular shape with a size of 10-30mm and a thickness from 0.5mm to several mm. The sample should be carefully ground down to 1000 grit. Finer grinding and polishing are not necessary.

Sample preparation for x-ray measurements

The sample surface is necessary to chemical etch or short electropolish to remove the deformation layers during sample preparation.

Sample preparation for special cases

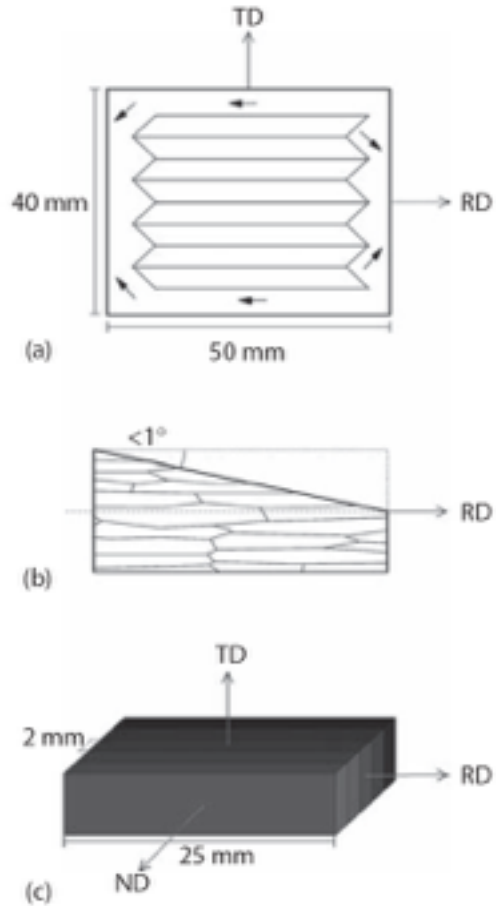

FIGURE 4.30
Measures to increase the sampling area during x-ray texture analysis. (a) Meander scan: The sample is translated in x and y direction, and at the end of each x-stroke of 42 mm, a lateral movement of 4 mm is carried out. After eight of these lateral shifts, the direction is reversed. (b) Sample with slightly slanted surface averaging over several through-thickness layers (not drawn to scale). (c) "Sandwich" sample stacked from several rotated pieces.